NTNU
Norwegian University of
Science and Technology

Parametric Excitation of Hangers at the Hardanger Bridge

Eirin Gundersen Lunde
Hans Andre Mangen Olsen

Civil and Environmental Engineering
Submission date: June 2016
Supervisor: Ole Andre Øiseth, KT
Co-supervisor: Daniel Cantero, KT

Norwegian University of Science and Technology
Department of Structural Engineering

Institutt for konstruksjonsteknikk

FAKULTET FOR INGENIØRVITENSKAP OG TEKNOLOGI
NTNU – Norges teknisk-naturvitenskapelige universitet

MASTEROPPGAVE 2016

for

Eirin Gundersen Lunde and Hans André Mangen Olsen

Parametric Excitation of Hangers at the Hardanger Bridge

Parametric excitation is a dynamic phenomenon that has been reported previously on hangers of suspension bridges. At the Hardanger Bridge large vibrations of some of the longest hangers have been observed. However, the cause of this large dynamic response has not been identified yet. It is believed that under certain conditions the traffic excites the bridge deck and the hangers in such a way that it induces parametric excitation. The goal of this project is to investigate the dynamic response of the hangers and confirm that the large vibrations are due to parametric excitation.

The project should cover following topics:

- Introduction to parametric excitation
- Previous experiences on similar bridges
- Numerical investigation of the bridge response
- Measurements on the Hardanger bridge
- Validation of numerical model
- Analysis of measurements
- Identification of the cause of high vibrations on hangers
- Evaluation of the consequences on the bridge's performance and lifespan

The project is organized according to the current guidelines

Supervisor(e): Ole Andre Øiseth, Daniel Cantero

NTNU, 18.01.2016

Ole Andre Øiseth
faglærer

Abstract

There has been observed large vibrations on some of the longest hangers at the Hardanger Bridge. Parametric excitation has been suggested as the cause of these vibrations. The main aim of this thesis has therefore been to verify if this is the case. As a preface to this inquiry, parametric excitation of cables has been looked into, and a search to find a numerical convergence criterion has been carried out. Though, without any concluding results.

The question of parametric excitation of the hangers at the Hardanger Bridge was first investigated by looking at numerical models of the hangers and the bridge. This was done to see if vibrations of the girder could excite the hangers. In addition to the question of parametric excitation, the dynamic properties of the hangers were sought. Experiments at the bridge were executed, rendering measurements to be utilized in modal analyses, and retrieving information to asses if parametric excitation could be a reasonable conclusion to the vibrations. Executed at the bridge were hammer tests and recordings of ambient vibration. Information of passing traffic was also retrieved to see if the traffic could excite the hangers. The dynamic properties were estimated using three modal analysis methods, i.e. circle fit, line fit and least-square complex exponential.

Based on the measurements from the Hardanger Bridge, circle fit and line fit could estimate reliable results for the natural frequencies. While the methods showed poor results for these measurements considering damping and mode shapes. Least-square complex exponential gave varying results for all the dynamic properties, and those re-

sults are therefore not presented.

Results from the numerical models indicated that parametric excitation due to girder vibrations was unlikely. While influence from traffic could be excluded after examining the ambient vibrations together with the traffic information. Concluding that parametric excitation is not probable, the ambient vibration data was inspected considering vortex shedding as the cause of the vibrations. Brief investigations indicated that this could be the case.

Sammendrag

Det har blitt observert store vibrasjoner på de lengste hengestengene på Hardangerbrua. Parametrisk eksitering er blitt foreslått som årsak til disse vibrasjonene. Hovedfokuset til denne oppgaven har derfor vært å verifisere om dette stemmer. Som en innledning til oppgaven er parametrisk eksitering av kabler blitt sett på. Undersøkelser for å finne et kriteria for når parametrisk eksitering inntreffer er blitt utført, men uten konkluderende resultater.

Spørsmålet om parametrisk eksitering av hengestengene på Hardangebrua ble først sett på med numeriske modeller av hengestengene og brua. Dette ble utført for å undersøke om vibrasjoner av brukassa kunne eksitere hengestengene. Det ble også etterspurt de dynamiske egenskapene til hengestengene i tillegg til årsaken til vibrasjonene. Som et tiltak ble eksperimenter på Hardangerbrua utført for å innhente resultater til modal analyser, og for å få informasjon til å evaluere om parametrisk eksitering er sannsynlig. Det ble utført *hammer tests* i tillegg til opptak av vibrasjoner og registrering av passerende trafikk. De dynamiske egenskapene ble estimert ved bruk av tre metoder; *circle fit, line fit* og *least-square complex exponentials.*

Basert på resultatene fra Hardangebrua, ga *circle fit* og *line fit* troverdige estimater for egenfrekvensene, men upålitelige resultater for demping og modeform. *Least-square complex exponentials* ga derimot varierende resultater for samtlige dynamiske egenskaper, og resultatene blir derfor ikke presentert.

Ut fra undersøkelsene på de numeriske modellene, tyder resultatene på at vibrasjoner

fra brukassa ikke vil forårsake parametrisk eksitering på hengestengene. Eksitering på grunn av trafikk kunne også utelukkes etter å ha sett på sammenhengen mellom vibrasjoner på hengestengene og passerende trafikk. Parametrisk eksitering ble derfor konkludert som lite sannsynlig. Vibrasjonene ble derfor undersøkt igjen, og overslags beregninger antyder at virvelavløsning er en mulig årsak til vibrasjonene.

Preface

This thesis represents the final work on our M.Sc. Degree at the Norwegian University of Science and Technology (NTNU). It was carried out between January and June 2016 at the Faculty of Engineering Science and Technology, Department of Structural Engineering. The master thesis has been supervised by Postdoc Daniel Cantero and Associate Professor Ole Øisteh, and in coopration with the Norwegian Public Road Administration.

The reader is assumed to have a background in structural engineering and good understanding of structural dynamics and FEM.

Eirin Gundersen Lunde
Hans André Mangen Olsen
Trondheim, June 6, 2016

Acknowledgment

We would like to thank our fellow M.Sc. students for making these five years very memorable, and a special thanks to those having to share an office with us this last semester while writhing our master thesis. Its been tedious but fun.

A big thank you to Postdoc Daniel Cantero for his generous support and an intriguing trip to the Hardanger Bridge. He was always fast at replying to emails and his general eagerness to assist has been highly appreciated. We would also like to thank Associate Professor Ole Øiseth for his contributions, and Professor Anders Rønnquist for his guidance during the fieldwork at the Hardanger Bridge.

Eirin Gundersen Lunde
Hans André Mangen Olsen
Trondheim, June 6, 2016

Contents

Acronyms

BC Boundary condition

CF Circle fit

FFT Fast Fourier transform

FT Fourier transform

FRF Frequency response function

IRF Impulse response function

LSCE Least square complex exponential

LF Line fit

MDOF Multi degree of freedom system

MIMO Multiple-input/multiple-output

NI National Instruments

PE Parametric excitation

PSD Power spectral density

SDOF Single degree of freedom

SISO Single-input/single-output

List of Figures

List of Tables

Chapter 1

Introduction

1.1 Background

As bridge connections at E39 on the western coast of Norway shall replace the ferry connections, longer and more optimized bridges need to be built. The dynamic properties of the bridges will be of major importance and research on special topics regarding the dynamic behavior are therefore highly relevant. This thesis will present the situation on the Hardanger Bridge regarding the vibrations on its longest hangers. Large vibrations on the longest hangers have been observed, with no clear reason for its cause. It is suggested that these vibrations are due to parametric excitation (PE), where traffic or wind induced vibrations of the girder, under particular frequencies, excite the hangers. This dynamic phenomenon has been reported on several cable stayed bridges, but fewer incidents on suspension bridges. Ben-Ahin Bridge and Wandre Bridge experienced amplitudes of more than 1m peak to peak and 30cm peak to peak in the first mode respectively. It is suspected that the cause was either rain-wind induced vibrations or PE causing the high amplitudes [11]. Farø Bridge in Denmark, Erasmus Bridge in Netherlands and Annacis Bridge in Canada have also had excitation of their stay cables [5]. Either mast or girder vibrations are said to be the cause of the induced cable vibrations. The theoretical derivation of the occurrence of PE is well determined from the Mathieu Hill equation [11], and clear theoretical boundaries for stable and unstable vibrations are determined from the harmonic balance method. PE

is highly sensitive to the amplitude initiated, causing exponential growth in vibrations within the unstable regions.

1.2 Structure and Approach of the Report

This thesis is presented to give the reader appropriate knowledge of the vibrations of the hangers on the Hardanger Bridge. The next chapter will include the theory of several techniques to extract the dynamic properties of a structure from the Frequency Response Function (FRF), with theory of relevant wind induced vibrations. The chapter will also include theory of hammer testing.

Chapter three presents a theoretical introduction into PE regarding cable excitation. Since the Hardanger Bridge is a suspension bridge the focus has only been on vertical cables with a small to no inclination. The modelling and simulations of the cables were executed in Abaqus, while the results were extracted and analyzed in MATLAB. The tension oscillations and the influence of damping will be investigated. A convergence criterion for stable and unstable displacements has not been performed numerically and an approach to find this will be presented. Based on this result, the criterion will be used to present a non-linear numerical stability chart. The convergence criterion will again be used to investigate PE of higher order modes.

In chapter four, the model of the Hardanger Bridge was investigated with respect to the possibilities for occurrence of PE. An Abaqus model of the Hardanger Bridge was provided by the Department of Structural Engineering and utilized to investigate the relation between the local modes of the hangers and the vertical modes of the bridge. Questioning if vibrations of the girder could excite the hangers.

Chapter five provides the procedure and setup of the experiment regarding the field-work executed on the Hardanger Bridge. Two types of experiments were performed. Ambient vibration tests were recorded at both girder and the two longest hangers. Hammer tests on the two longest hangers were executed, and the dynamic proper-

ties and cable tensions were extracted from those tests. The ambient vibration results were used to check the influence from traffic and wind. The hammer tests have been analyzed with EasyMod in MATLAB, while the ambient tests were analyzed directly in MATLAB.

The final chapter, presents the concluding remarks from our experiments with a discussion of the consequences of the vibrations. Additional information on the cables, detailed description of the setups from the fieldwork and essential MATLAB scripts are given in the appendixes.

Chapter 2

Theory

In this chapter some modal analysis techniques will be presented, coupled with some basic theory regarding structural dynamics and Fourier analysis. The modal analysis techniques will be utilized later in this thesis on results from hammer tests, also explained in this chapter. In addition to some relevant theory on wind induced vibrations, proposing an alternative cause for the vibrations for discussions in the concluding chapter.

2.1 MDOF in the Time Domain

The equation of motion is usually given in the time domain. For a system with multiple degree of freedom (MDOF), the equation then renders [17]:

$$[M][\ddot{y}(t)] + [C][\dot{y}(t)] + [K][y(t)] = [f(t)] \tag{2.1}$$

Where $[f(t)]$ is the external force on the system. The matrixes $[M]$, $[C]$ and $[K]$ are the mass-, damping- and stiffness matrix, respectively. $[y(t)]$, $[\dot{y}(t)]$ and $[\ddot{y}(t)]$ are successively displacement, velocity and acceleration. By solving the differential equation, the mode shapes and corresponding natural frequencies and damping ratios can be determined. The general solution to the equation is given by [17]:

$$[y(t)] = [a]e^{i\omega t} \tag{2.2}$$

Where $i = \sqrt{-1}$. Inserting equation 2.2 and its derivatives in equation 2.1, the equation renders:

$$\left\{-\omega^2[M] + i\omega[C] + [K]\right\}[a] = [f(t)] \tag{2.3}$$

2.2 MDOF in the Frequency Domain

The dynamic properties of a system can also be analyzed in the frequency domain. Here the equation of motion is a set of algebraic equations. By use of a Fourier transform (FT), the signal in the time domain can be converted to the frequency domain. FT is explained further in section 2.3. The equation of motion in the frequency domain then yields [17]:

$$\left\{-\omega^2[M] + i\omega[C] + [K]\right\}[Y(\omega)] = [F(\omega)] \tag{2.4}$$

Where $[Y(\omega)]$ and $[F(\omega)]$ are the FT of $[y(t)]$ and $[f(t)]$, respectively. The relation between the response and the external force is the FRF, denoted $[H(\omega)]$ [17]:

$$[H(\omega)] = -\omega^2[M] + i\omega[C] + [K] = \frac{[Y(\omega)]}{[F(\omega)]} \tag{2.5}$$

The FRF can take different forms, depending on the response extracted from the system. Receptance, mobility and accelerance for displacement, velocity and accelerations respectively, and the relation between them is $i\omega$.

2.3 Fourier Analysis

2.3.1 Fourier Transform

As mentioned, a signal in the time domain can be converted into the frequency domain with a FT. The FT can be defined as follows [24]:

$$F(\omega) = \frac{1}{\sqrt{2\pi}} \int_{-\infty}^{\infty} f(t) e^{-i\omega t} dt \tag{2.6}$$

The inverse transform renders:

$$f(t) = \frac{1}{\sqrt{2\pi}} \int_{-\infty}^{\infty} F(\omega) e^{i\omega t} dt \tag{2.7}$$

2.3.2 Fast Fourier Transform

A Fast Fourier transform (FFT) computes the discrete FT of a signal. The discrete transformation approximates an infinite series with infinite values into a definite series. The sum renders [24]:

$$X_k = \frac{1}{N} \sum_{n=0}^{N-1} x_(n) e^{-i\frac{2\pi}{N}kn} \tag{2.8}$$

Where x_n are the values in the time domain with $n = 0,\ldots, N\text{-}1$. X_k are the computed values in the frequency domain with $k = 0,\ldots, N\text{-}1$.

The time domain values are recorded with a constant interval Δt over a total time T. Number of recorded values then yields $N = \Delta t * T$. Thus rendering a sampling frequency $f_s = \frac{1}{\Delta t}$ and frequency step $\Delta f = \frac{1}{T}$. Because of this correlation, one needs an adequate long signal to get sufficient resolution in the frequency domain. The invers transformation renders [24]:

$$x_n = \frac{1}{N} \sum_{n=0}^{N-1} X_k e^{-i\frac{2\pi}{N}kn} \tag{2.9}$$

2.4 Rayleigh Damping

Rayleigh damping is based on the simple hypothesis that wherever there is a contribution from mass or stiffness to a system, there will also be energy dissipation. Rayleigh damping therefor utilizes a method where viscous damping is introduced as a percentage of the systems critical damping. The damping matrix is then a linear combination of the stiffness and mass matrix [17]:

$$[C] = \alpha[M] + \beta[K] \tag{2.10}$$

Developing the modal damping matrix from the orthogonality properties of the mode shapes renders [17]:

$$[\tilde{C}] = [\phi]^T[C][\phi] = \alpha[\phi]^T[M][\phi] + \beta[\phi]^T[K][\phi] = \alpha[\tilde{M}] + \beta[\tilde{K}] \tag{2.11}$$

$$= diag\left[\alpha[\phi_n]^T[M][\phi_n] + \beta[\phi_n]^T[K][\phi_n]\right] = diag\left[\tilde{M}_n(\alpha + \beta\omega_n^2)\right] \tag{2.12}$$

Comparing it to the damping matrix of type [17]:

$$[\tilde{C}] = diag\left[2\tilde{M}_n\omega_n\zeta_n\right] \tag{2.13}$$

Gives $\left[2\tilde{M}_n\omega_n\zeta_n\right] = \left[\tilde{M}_n(\alpha + \beta\omega_n^2)\right]$, rendering the damping, ζ_n, for a natural frequency of mode n as:

$$\zeta_n = \frac{1}{2}\left(\alpha\omega_n^{-1} + \beta\omega_n\right) \tag{2.14}$$

Figure 2.1 visualize the Rayleigh damping curve for $\zeta_1 = \zeta_2 = 2\%$ at $1Hz$ and $2Hz$ respectively. Given two natural frequencies with corresponding damping, the constants α and β can be determined [17]:

$$\alpha = \frac{2\omega_1\omega_2(\omega_2\zeta_1 - \omega_1\zeta_2)}{\omega_2^2 - \omega_1^2} \tag{2.15}$$

$$\beta = \frac{2(\omega_2\zeta_2 - \omega_1\zeta_1)}{\omega_2^2 - \omega_1^2} \tag{2.16}$$

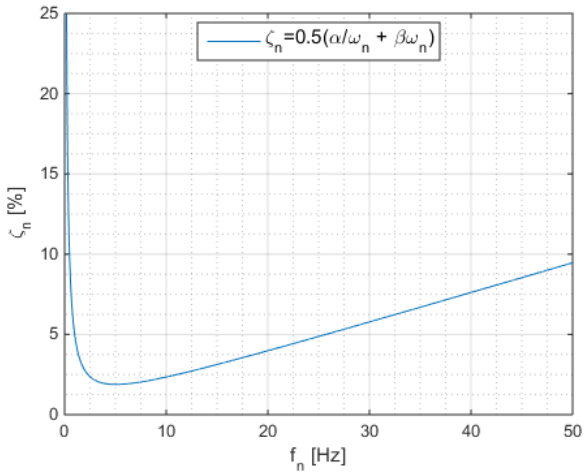

Figure 2.1: Rayleigh damping curve for $\zeta_1 = \zeta_2 = 2\%$ at 1Hz and 2Hz.

2.5 Mersenne's Law

The equation explaining the relation between the natural frequency and tension in a string is known as Mersenne's law. When knowing the properties of the string, the natural frequencies of mode n can be calculated as follows [15]:

$$f_n = \frac{n}{2L}\sqrt{\frac{T}{\mu}} \tag{2.17}$$

Where L is the length of the string in $[m]$, T the tension in $[N]$ and μ the linear density in $[kg/m]$.

2.6 Hammer Testing

A technique to extract modal parameters from a system is modal hammer testing. It is a well used technique since it is portable and therefore convenient for fieldwork. The technique requires a modal hammer, an accelerometer, a dynamic module and a computer.

The hammer consist of a changeable impact tip and a wire connected at the bottom of the shaft, which leads the impulse signals to the dynamic module. To have control over the force level one needs a heavier hammer when hitting a larger structure. The bandwidth of the frequency is inverse proportional to the duration of the pulse, and the duration of the pulse and magnitude depends on the dynamics of the structure surface. Frequency bandwidth is also dependent on the material of the hammer tip and the velocity at impact. If a high frequency content is desired, a harder hammer tip should be used to shorten the pulse duration [9, 21].

The triaxial accelerometers, used later in the fieldwork, are piezoelectric accelerometers. They are built as a mass-spring. The piezoelectric element works as a spring and damper, where the accelerations applied on the accelerometer is transferred to the spring. These accelerations are absorbed by the piezoelectric element, which sends

out a voltage proportional to the acceleration [2].

Using the hammer to measure the input and the accelerometer to measure the output, the FRF can be estimated. This function of frequency now describes the relation between the point where the hammer excited the structure and the point where the accelerometer was attached. Moving either the point where the accelerometer is attached or where the hammer excites the structure, the FRF of the whole structure can be estimated. The more points one has the relation between, the closer the estimate gets to represent the structure correctly.

2.7 Modal Analysis Methods

Over the last decades there has been developed several techniques to extract dynamic properties. These techniques can be classified as time domain or frequency domain methods. Three techniques will be presented in this thesis as they will be utilized later to extract the dynamic properties of the hangers. Circle fit (CF) and line fit (LF) are both frequency domain methods and least-squares complex exponential (LSCE) is a time domain method. The two frequency domain methods utilized were both SISO methods. FRFs from several simulations were summed up to one FRF in order to use the SISO methods. LSCE is a MIMO method, and the advantage of MIMO methods is the capability to handle several FRFs at the same time. Variations in the different FRFs will then be averaged out, due to the assumption that damping ratio and natural frequencies are global properties of the structure [12].

2.7.1 Circle Fit

The motive of the CF method is to extract natural frequencies, damping loss factors and modal constants from a reference circle called Nyquist plot. The Nyquist plot make use of the FRF, and it can be used on both SDOF and MDOF systems. If the CF method is to be used on a MDOF system, it is under the assumption that around resonance the contribution from one mode is dominant compared to all other modes, and thus neglects

them. The FRF is a complex function, and the real, imaginary and frequency part are therefore needed to fully represent the FRF [12].

Taking the projection of the FRF into the complex plane one gets a circular loop, and it is this circularity the CF method relies on. In a MDOF system the FRF will have several peaks, and consequently a limited number of data points are used. The Nyquist plot will therefore consist of a part of a circle, and not a complete one, since the total signal is not projected. The natural frequency is extracted from the Nyquist plot by finding the location of the maximum arc change. For a mathematically derivation of extracting the natural frequency see [6]. The derivation leads to the following equation:

$$\omega^2 = \frac{1+\sqrt{1+3(1+\eta^2)}}{3}\omega_r^2 \tag{2.18}$$

Where η and ω_r are the damping loss factor and resonance frequency. When the damping loss factor is sufficiently small equation 2.18 leads to the resonance frequency.

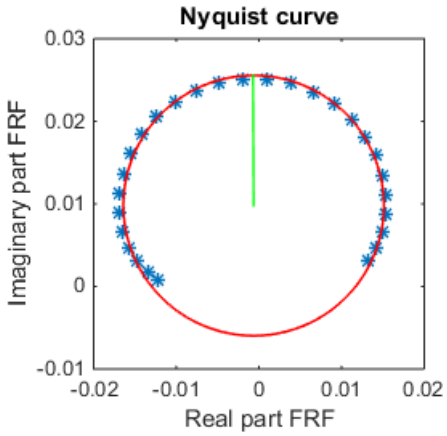

Figure 2.2: Generated FRF on Nyquist curve

Estimating the damping loss factor can be done by taking two points on the circle, ω_a and ω_b, that lies on each side of ω_r. The angle between their location and ω_r then

determines the damping loss factor by the following equation [6].

$$\eta = \frac{\omega_a^2 - \omega_b^2}{\omega_r^2} * \frac{1}{tan\frac{\theta_a}{2} + tan\frac{\theta_b}{2}} \tag{2.19}$$

Figure 2.2 represents points around resonance from a FRF drawn on a perfect circle, where the green line denotes the location of ω_r.

2.7.2 Line Fit

Instead of a curve fit of the FRF it is possible to use the linearity of the inverse FRF to make a LF of the FRF. By looking at the r-th peak of the FRF, the receptance with structural damping can be stated as [6]:

$$\alpha_{jk}(\omega) = \frac{{}_rA_{jk}}{{\omega_r}^2 - \omega^2 + {\omega_r}^2\eta_r i} \tag{2.20}$$

Where ω_r is the resonance frequency and A_r is a modal constant of the mass-normalized mode shape matrix, $[\Phi_j\Phi_k]$, for the r-th mode. Looking at a frequency, Ω, near ω, and taking the difference of their inverse FRF and rearrange, one obtain a new function with respect to ω^2. Introducing the complex natural frequency square as:

$${\lambda_r}^2 = {\omega_r}^2(1 + {\eta_r}^2 i) \tag{2.21}$$

The new function can be expressed as [12]:

$$\Delta = \frac{({\lambda_r}^2 - \omega^2)({\lambda_r}^2 - \Omega^2)}{{}_rA_{jk}} \tag{2.22}$$

This equation can be divided into a real and an imaginary part, where both equations will be linear functions of ω^2. Selecting different frequencies around ω_r one gets slopes with different inclination as in figure 2.3. The resonance frequency will then be found at the point on ω^2-axis where the lines intersect.

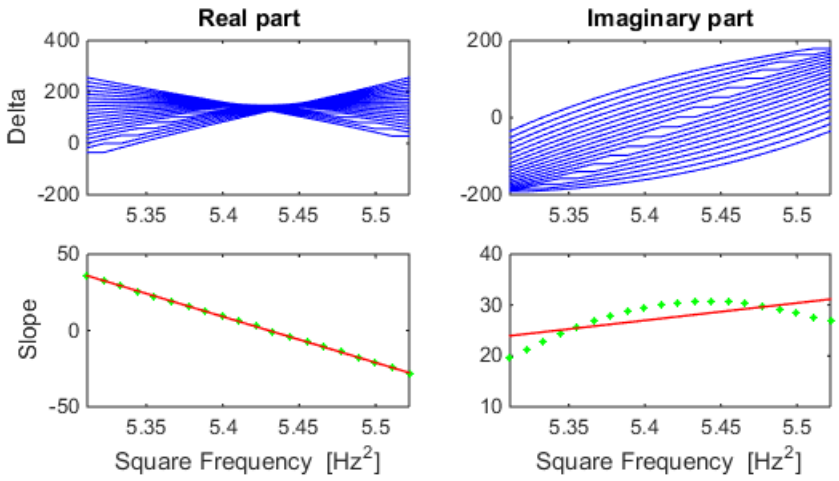

Figure 2.3: Line fit method. Slopes and delta function

2.7.3 LSCE

The LSCE method is a time domain method analyzing numerous of impulse response functions (IRF) for each analysis, where the IRF is calculated from the inverse of the FT. The idea behind the LSCE method is to combine the impulse at several points and the measured response at several locations to extract damping ratios, natural frequencies and mode shapes. The method is highly dependent on number of modes considered in the analysis. The analysis can be performed several times, decreasing the number of modes for each time. Comparing the error between the reproduced signals and the original signal, there should be an evident decrease in error for the right number of modes. Another disadvantage is the sensitivity of the signal to noise ratio. The entire signal is used to extract the modal parameters and consequently one does not have the possibility to search around a resonance peak as in CF and LF. Figure 2.4 visualize a

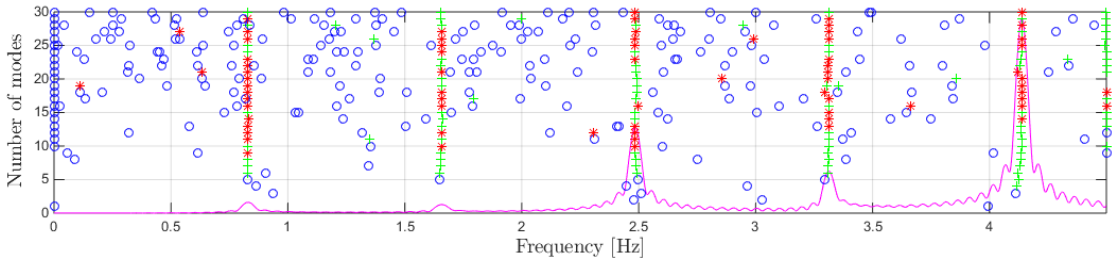

Figure 2.4: Stabilization diagram from LSCE. The blue circle indicate a new mode. The green cross indicate frequency stabilization and the red crosses indicate frequency-damping stabilization.

stabilization diagram produced by the LSCE method in EasyMod in MATLAB. The corresponding error chart for number of modes to choose in order to extract the dynamic properties is given in figure 2.5 [12].

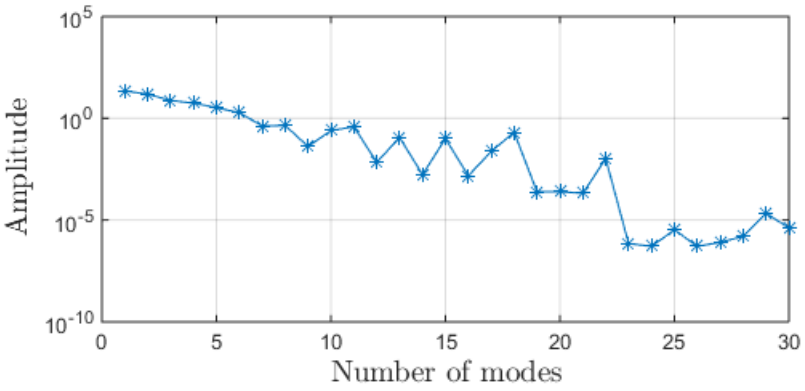

Figure 2.5: LSCE error chart

2.8 Vortex Shedding

When fluids floats by an object at a certain velocity, the fluid will start to oscillate behind the object. This oscillating of fluid will induce low-pressure zones, which the object will move towards. This is called vortex shedding, and the frequency for which it occurs is described by [16]:

$$f_s = \frac{S_t v}{D} \tag{2.23}$$

Where f_s is the shedding frequency, S_t is the Strouhal number, D is the diameter of the structure and v is the velocity of flow on the structure. The Strouhal number have been investigated by several researchers, and measured to $S_t = 0.19$ for Reynolds number lower than $2 * 10^5$ for a circular cylinder [18, 22].

Chapter 3

Parametric Excitation

3.1 Theory

PE is a non-linear effect, where oscillations are driven by varying a parameter of the system at some frequency. The frequency of the excitation is usually away from the linear natural frequencies of the system, and even a small PE can produce a large response [14]. The mathematical background for PE is based on the Hill equation. The general Hill equation is a linear second order differential equation of type [7]:

$$\ddot{y}(t) + f(t)\,y(t) = 0 \tag{3.1}$$

Where $f(t)$ can be spanned into Fourier series. Thus obtaining the following differential equation:

$$\ddot{y}(t) + \left(A_0 + \sum_{n=1}^{\infty} A_n \cos(2\upsilon n t) + \sum_{m=1}^{\infty} B_m \sin(2\upsilon m t)\right) y(t) = 0 \tag{3.2}$$

The simplest form of equation 3.1 is the Mathieu Hill equation, where only one harmonic mode is considered. This renders [11]:

$$\ddot{y}(t) + (a + P\cos(2\upsilon t))\, y(t) = 0 \tag{3.3}$$

Where $a = A_0$, $P = A_1$, $A_{n+1} = A_{n+2} = ... = 0$ and $B_{m+1} = B_{m+2} = ... = 0$.

PE for a cable occurs when the cable is subjected to a periodic movement at one cable end, which then induces tension oscillations in the cable. For specific frequencies, this periodic effect on the stiffness can develop large transverse displacements with exponential growth. The amplitude of the displacements is barely influenced by damping, only limited by non-linearities.

Identifying when this instability occurs is of great importance. So called transition curves define the boundaries dividing the stable from the unstable cases. The harmonic balance method is one way to theoretically compute these instability regions. In this thesis the transition curves are not computed theoretically, but they are investigated numerically, see section 3.3.2. The harmonic balance method is elaborated in [19, 20]. Increasing the excitation amplitude will expand the unstable regions very quickly. Thus for large excitation amplitudes almost all frequency ratios between zero and 2.5 will be unstable. Frequency ratio is the ratio between the excitation frequency and the cable's natural frequencies $\frac{\omega_{exc}}{\omega_s}$ [11].

For a cable subjected to a periodic anchorage movement the Mathieu Hill differential equation can be solved by the method of separation of variables and gives the transverse movement, $w(x,t)$, of the cable [11]:

$$w(x,t) = \sum Y_s(t) W_s(x) \tag{3.4}$$

Where $Y_s(t)$ is the amplitude and $W_s(x)$ is the sth mode shape.

The Irvine parameter, γ^2, is a fundamental non-dimensional parameter that accounts for the geometric and elastic effects in the cable behaviour. The Irvine parameter governs [8, 11]:

$$\gamma^2 = \left(\frac{mgl}{H}\right)^2 l * \left(\frac{HL_e}{EA}\right)^{-1} \tag{3.5}$$

Where m is mass per unit meter, g is the ground acceleration, l is the cable length, H is the horizontal component of the cable tension, E is Young's modulus, A is the

cross-section of the cable, and L_e is given in equation 3.6, with reference to figure 3.1:

$$L_e = l\left\{1 + \frac{1}{8}\left[\frac{mgl}{H}\right]^2\right\} \tag{3.6}$$

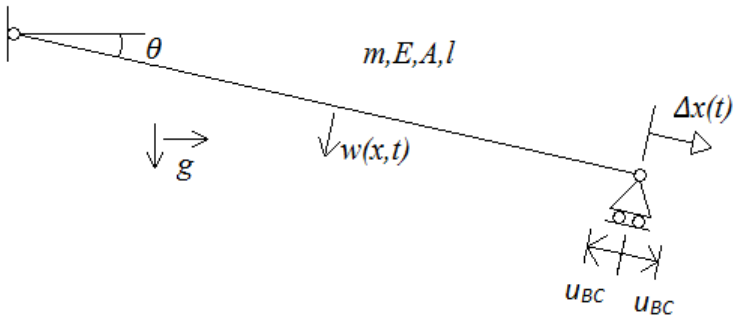

Figure 3.1: Typical cable with boundary conditions

For stay cables, or vertical cables as on suspension bridges, γ^2 is small because the sag/span ratio is small. So when calculating the $W_s(x)$ the eigenfunctions of a taut string is used.

When the excitation amplitude is small, the unstable cable movement can occur close to the following excitation frequencies, given the simple case of PE with only one harmonic mode:

$$\omega_{exc} = 2\upsilon = \frac{2\omega_s}{k} \tag{3.7}$$

For all k and where ω_s is the natural frequency of the cable in mode s. When the movement becomes unstable the displacement starts to grow exponentially.

3.2 Case Study: PE in Abaqus

Further investigation of PE in this chapter will be from a numerical perspective. A cable was modelled to investigate the influence of damping and the tension oscillations during PE. Modelling and simulation of the cable was done with MATLAB and Abaqus, taking origin in the hangers at the Hardanger Bridge. The cable was modelled with B21

elements to get transverse displacement and was pinned at both ends with a relative vertical displacement of 1% of the length at one end. The angle of the cable to the global axis was therefore 0.57 degrees, which gives the cable transverse and horizontal response. A cyclic boundary displacement in horizontal direction was set at the end of the cable to force the cable into PE. An initial temperature stress was included to imitate the prestress in the hangers, rendering the natural frequencies of the cable to be higher than originally. Since the cable was modelled with basis in the hangers at the Hardanger Bridge, the cable was given properties as those. The properties can be found in table 4.1 in chapter 4.

3.2.1 PE Simulations

Modelling a 100m long cable with geometry and properties as mentioned above, the natural frequencies were extracted before subjecting the cable to the periodic boundary condition (BC). The temperature was set to -143 degrees, which is equal to an initial stress of roughly 275MPa. This stress correspond with the measured load retrieved from the technical drawings of the Hardanger Bridge, provided by the Norwegian Public Roads Administration [1]. The periodic BC was modelled by a sine wave, $u_{BC}\sin(2\omega_s t)$, where ω_s is the cable's natural frequency in mode s in $[rad/time]$. In the simulation u_{BC} was set to 0.05m and the simulation was executed for 50s. The displacement of mid node is visualized in figure 3.2a. Tension oscillation for mid element is shown in figure 3.2b.

No damping was included in the simulation, but the influence from damping will be looked at in a later simulations. The cable in figure 3.2 is evidently in parametric resonance at an excitation frequency twice the fundamental frequency, seeing as the transverse displacement grows exponentially until it reaches maximum displacement of an amplitude close to 1.5m. Looking at the tension oscillations it is clear that the mean tension increases as the displacement grows, and when the displacement is at its maximum, the tension oscillations tends to zero close to the maximum initial value. This is seen more clearly in fig 3.3.

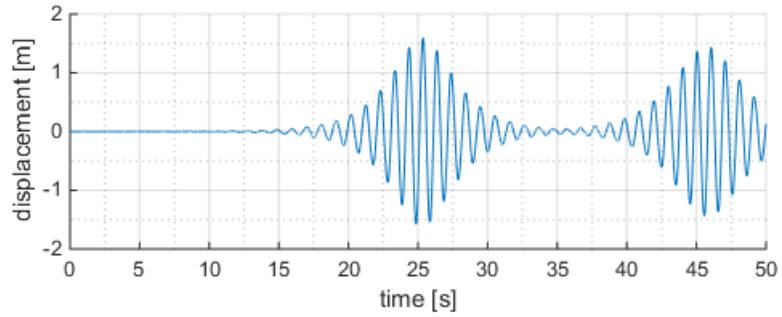

(a) Transverse cable displacement of mid node

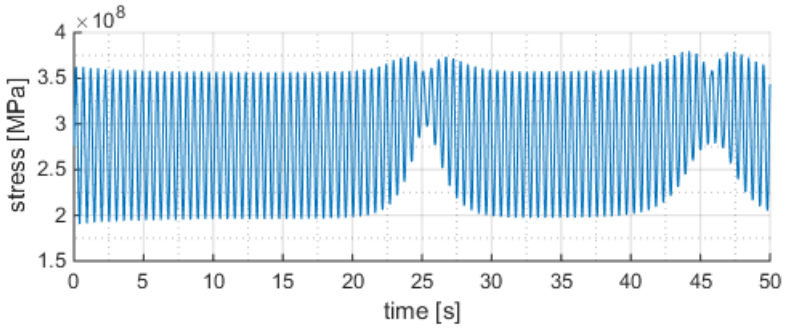

(b) Tension oscillation in mid element

Figure 3.2: PE in cable excited at twice the fundamental frequency

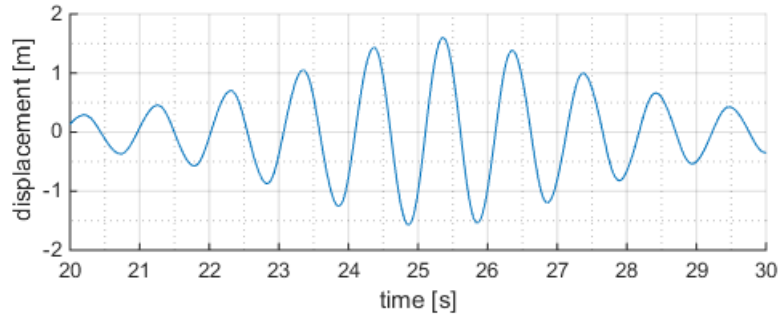

(a) Detail of figure 3.2a

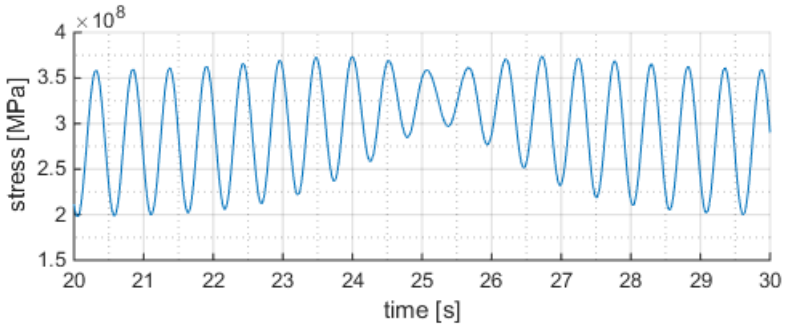

(b) Detail of figure 3.2b

Figure 3.3: Detail of figure 3.2

In figure 3.4 the same cable is simulated included damping. The damping is set as Rayleigh damping, with 2% damping at the fundamental frequency and equivalently at twice the fundamental frequency. Comparing the simulation, with and without damping, there is no significant difference in magnitude for either displacement or stress. When looking closer at the graphs concerning displacement, it is evident that the damping influences the point of onset of PE, and keeps the displacement from tending back to zero before PE again initialize. For the tension oscillation, the damping increases the lower bound stress after the first onset of PE.

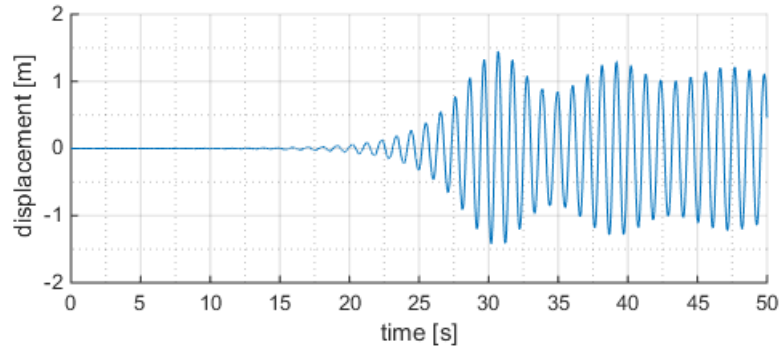

(a) Transverse cable displacement at mid node

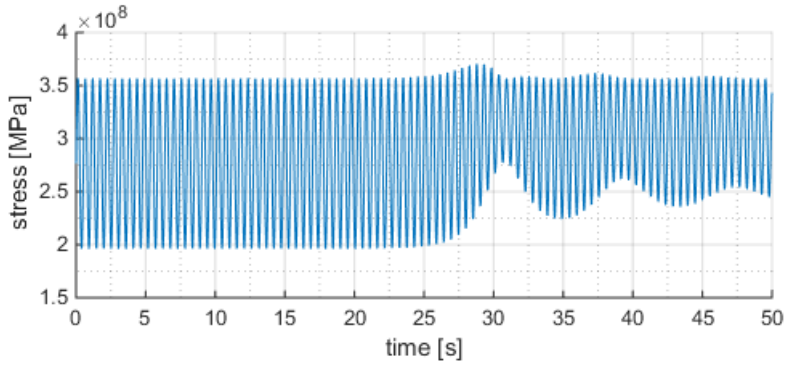

(b) Tension oscillation in mid element

Figure 3.4: PE in cable excited at twice the fundamental frequency, with damping

3.3 Numerical Analysis

During this thesis there has been a search to find a convergence criterion for occurrence of PE. The harmonic balance method gives clear theoretically transition curves, but no clear definition with respect to numerical solutions. Simulations have been executed in the search to find a convergence criterion for PE. These simulations were

carried out to see if there were any parameters that are decisive for the development of PE, and how the stabilization chart would be with those criteria. The ratio between maximum transverse displacement, u_c, and the cyclic BC displacement, u_{BC}, has been mentioned in other papers [11, 25], and was looked further into. The stability chart was produced for the fundamental frequency based on the results from the ratio analysis and from previous analysis performed in *Parametric excitation of mooring cables for submerged floating tunnels* [3]. The last analysis presented in this section is on PE of higher order modes. The analysis presents the time before unstable transverse displacements, $u_c > u_{BC}$, occur for different amplitudes.

3.3.1 Stable and Unstable Vibrations

In the search to find a numerical convergence criterion for occurrence of unstable vibrations, the ratio between u_c and u_{BC} was investigated. To inspect the ratio between $\frac{u_c}{u_{BC}}$, five different lengths between $10m$ and $60m$ were chosen. Since PE of the first mode is the most critical, the lengths were chosen such that the fundamental frequency of one cable would not coincide with a multiple of natural frequencies of the other lengths. Lengths with their corresponding fundamental frequency are shown in table 3.1. The respective cables were driven by a cyclic amplitude, u_{BC}, at the cable

Length [m]	Eigenfrequency [rad/s]
11	54.087
23	25.749
32	18.495
41	14.431
53	11.162

Table 3.1: Lengths and natural frequency of respective cables

end. The excitation amplitude, u_{BC}, was normalized by dividing it with the length of the cable, $\frac{u_{BC}}{L}$, and each cable was then driven by the normalized amplitudes. The plots in figures 3.5a to 3.5e shows the normalized maximum displacement for each length. In the paper *Parametric excitation of mooring cables for submerged floating tunnels* [3], transition curves and numerical analysis are plotted together. It is there showed that when the ratio of maximum transverse displacement and the excitation

amplitude is equal to one, the numerical solutions are close to the transition curves. Figure 3.5f displays the normalized amplitude on the vertical axis and the different lengths on the horizontal axis. The red crosses specify that $\frac{u_c}{u_{BC}} > 1$ and blue circles specify that $\frac{u_c}{u_{BC}} <= 1$. Figure 3.5 shows that a small increase in $\frac{u_{BC}}{L}$ leads to a major growth of the maximum transverse displacement. Although there is no clear limit

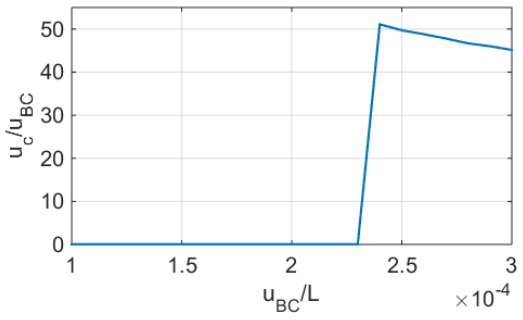

(a) Normalized displacement for $L = 11m$

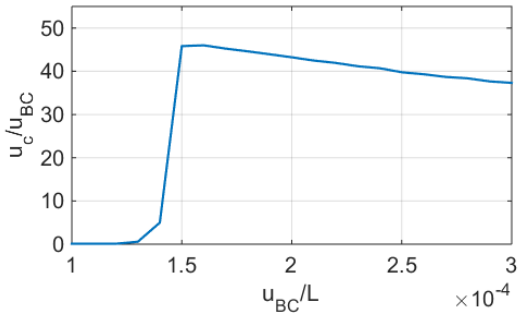

(b) Normalized displacement for $L = 23m$

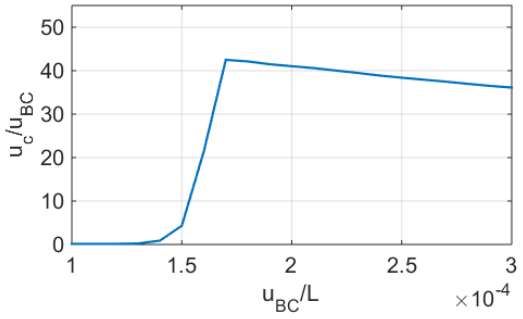

(c) Normalized displacement for $L = 32m$

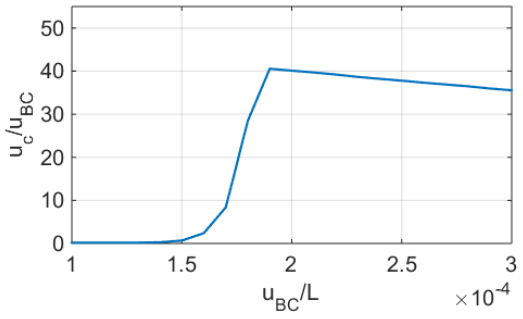

(d) Normalized displacement for $L = 41m$

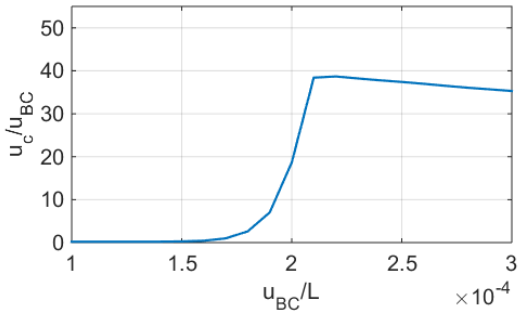

(e) Normalized displacement for $L = 53m$

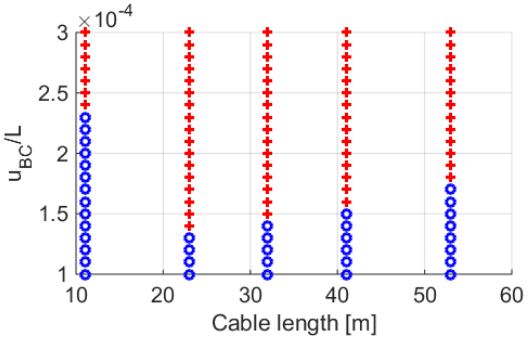

(f) Normalized amplitude for the five cables

Figure 3.5: Figure (a) to (e) shows the normalized displacement against the normalized excitation amplitude. The red crosses in (f) indicate unstable displacement, and blue dots otherwise.

for when unstable vibrations occur, large maximum displacement occurs close after $\frac{u_c}{u_{BC}} > 1$ for all lengths. The difference in normalized excitation amplitudes, seen in figure 3.5f, with this criteria is slight, and therefore utilized in further tests.

3.3.2 Stability Chart

On the basis of the unstable displacement criterion, $\frac{u_c}{u_{BC}} > 1$, a stability chart was made. A $23m$ long cable, modelled with B21 elements, was initiated with amplitudes from $0.1cm$ up to $4.5cm$. These cyclic amplitudes excited the cable with a frequency of 0.1 up to 2.5 times its fundamental frequency. From the harmonic balance method one gets transition curves where the boundary between stable and unstable displacements lies at the border of those curves. The stability chart shown in figure 3.6 indicate that there are similarities to the transition curves, but not as clear as transitions curves from the harmonic balance method. The red crosses in figure 3.6 indicate that $\frac{u_c}{u_{BC}} > 1$, and

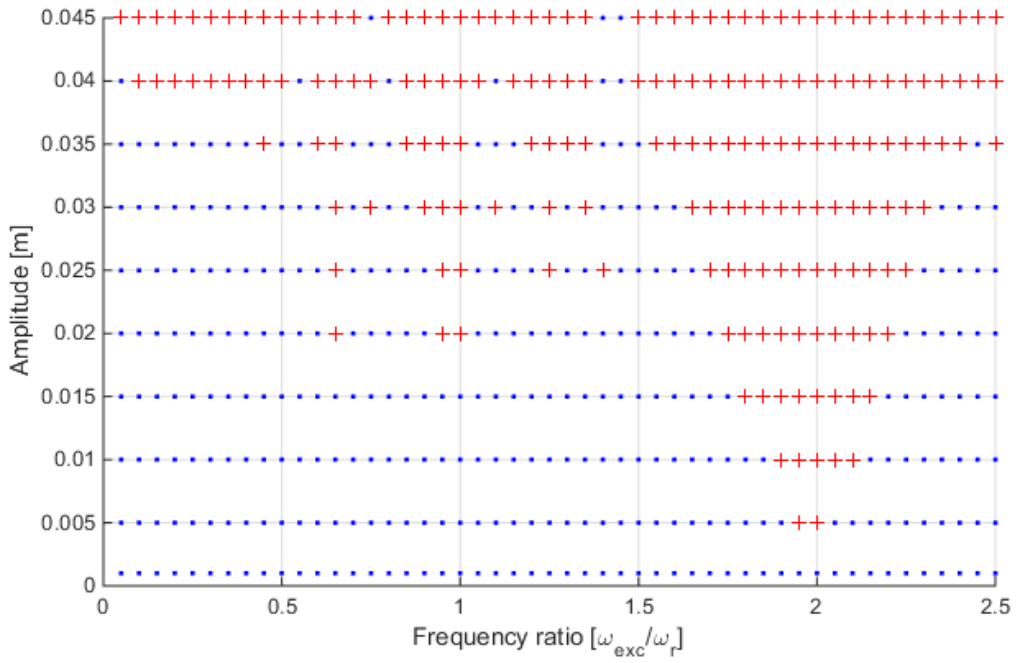

Figure 3.6: Stability chart. Blue dots indicate stable vibrations and red crosses indicate unstable vibrations.

the blue dots otherwise. The simulations were executed without damping to visualize the full effect of PE. According to the Mathieu Hill theory there should have been unstable vibrations for any excitation amplitude at twice the natural frequency. It is important to emphasize that for larger excitation amplitudes unstable vibrations occur for all frequencies. The stability chart in figure 3.6 indicate that unstable vibrations occur for low amplitudes at $k = 1, k = 2$ and $k = 3$. This emphasize the theory in section 3.1, that unstable PE exist for any k. However, the Mathieu Hill equation point to unstable

PE for excitation amplitudes lower than those evident in figure 3.6. This would be the case if damping was included [11], but the stability chart was made without including damping in the simulations. This could indicate that the unstable displacement criterion is to strict compared to the theoretical transition curves. The non-linear effect in the simulations could also be the cause of no unstable PE for excitation amplitudes lower than $0.02m$ for $k = 2$ and $k = 3$.

3.3.3 Excitation of Higher Modes

To relate the previous results to the experiments executed on the Hardanger Bridge, investigation of unstable PE for higher order modes were carried out. The cable was modelled with the same properties as previous simulations and the length of the cable was set to $100m$, similar to the longest hangers at the Hardanger Bridge. The first 10 modes were extracted from Abaqus and set as half the frequency for u_{BC}. Three different cyclic BC amplitudes, $0.04m$, $0.07m$ and $0.10m$, were initiated in global horizontal direction at the cable end. The simulations were done with and without damping. The frequencies for the Rayleigh damping were set to be the fundamental and twice the fundamental frequency, with 2% damping for both frequencies. Figure 3.7 shows the time before onset of PE, set to $u_c > u_{BC}$. Figure 3.7a is without damping and one can see that the time needed before unstable PE occur is shorter than for figure 3.7b, included damping. This is expected, but for mode 2 and 3 the difference is very little. For the four highest modes, the damping is a significant factor to delay the excitation for the lowest excitation amplitudes. The initiation of PE for the two highest amplitudes is not significantly affected of the damping, and the time before unstable PE occur is close to $1s$ for the four highest modes, with and without damping. This indicate that a PE would occur if the excited amplitude and damping ratio is of such magnitudes. Figure 3.7 clearly visualize that one need the same ongoing frequency over several seconds if the excitation amplitude is of a lower magnitude.

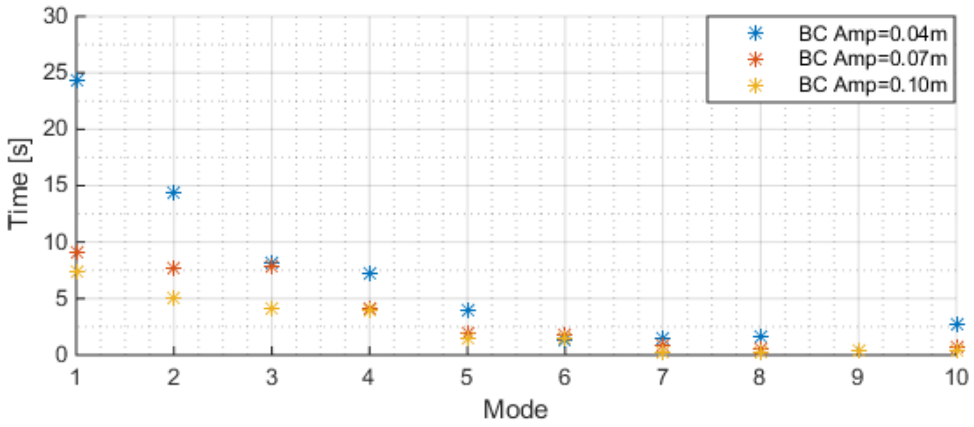

(a) Unstable PE for the 10 first modes with no damping.

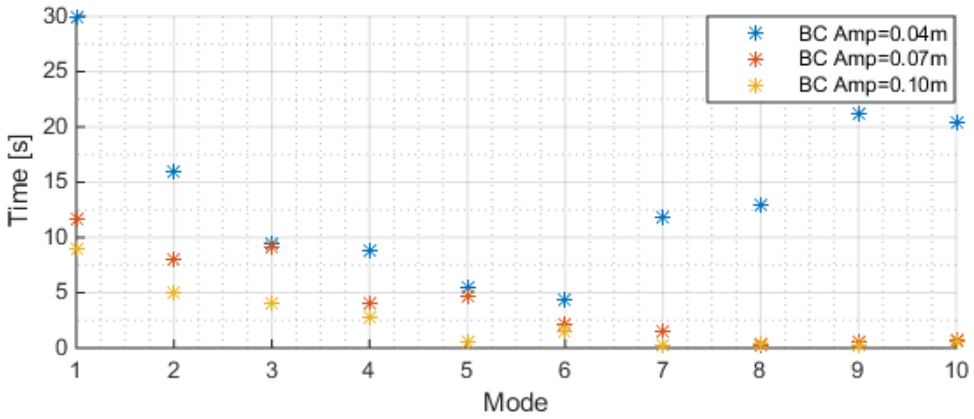

(b) Unstable PE of the 10 first modes with 2% Rayleigh damping

Figure 3.7: The markings illustrate the time when $u_c > u_{BC}$ for their respective amplitudes.

Chapter 4

Hardanger Bridge

The Hardanger Bridge is a 1320m long suspension bridge connecting the parishes Vallavik and Bu. The bridge was built over a period of four years. Construction of the bridge started 26. of February 2009 and ended 17. of August 2013, making it the longest suspension bridge in Norway. The bridge consists of one girder span between two pylons and hangers connected in between. The pylons were made of concrete, rising over 200m above sea level, standing on solid ground on each side of the Eidfjord. The two main cables consist of 19 strands, each containing 528 steel wires, each wire with a diameter of 5.3mm [23]. Hangers are placed at a distance of 20m along the girder. The hangers have different lengths, varying from 3m up to 127m, with spiral-laid wires except for the five shortest hangers, which were made of one cast steel. The girder was made of steel sections, which were bolted and welded at site after connected to the hangers [1].

4.1 Abaqus Model

A pre-existing Abaqus model of the whole bridge, provided by the Department of Structural Engineering, was used when looking at the Hardanger Bridge's natural frequencies. The accuracy of this bridge model was not verified in this thesis, but still utilized as the model was assumed an adequate representation. The bridge model was used to verify if vibrations of the girder could excite the hangers into PE. Assuming that both frequencies from the modelled hangers and bridge are relatively in accordance with

the actual bridge.

4.1.1 Hangers

Looking more specific into the hangers at the Hardanger Bridge, all 30 hangers were modelled in Abaqus. The hangers were modelled as beams, using B21 elements, and the beams were pinned at both ends. The hangers were modelled with properties retrieved from technical drawings provided by the Norwegian Public Roads Administration [1]. Properties not specified in technical drawing were retrieved from other references listing steel properties [4, 10]. See table 4.1.

Property	Value
E-modulus $[N/m^2]$	$160 * 10^9$
G-modulus $[N/m^2]$	$61.5 * 10^9$
Radius $[m]$	0.0319
Thermal expansion coefficient $[K^{-1}]$	$1.2 * 10^{-5}$
Density $[kg/m^3]$	7850

Table 4.1: Hanger properties

The pre-tensioning in the hangers was obtained by applying temperature to induce thermal stresses. The temperatures set were calculated from the measured applied load specified in technical drawings. The corresponding tension and length for the two longest cables are presented in table 4.2 [1]. After the hangers were modelled with these properties, a frequency step was calculated rendering the 20 first natural frequencies for each hanger. The first ten natural frequencies for the two longest hangers are listed in table 4.3. In appendix A lengths and measured loads from technical drawings for all 30 hangers are listed, together with the first 20 natural frequencies for each hanger. Frequencies retrieved from Abaqus are not completely linear, as Mersennes's law presented in section 2.5 states. This deviation is presumably due to the non-linearities included in the model.

	Hanger 1	Hanger 2
Length $[m]$	127.531	119.749
Tension $[kN]$	980	983

Table 4.2: Length and tension in Hanger 1 and 2

Mode	Hanger 1	Hanger 2
1	0.774	0.826
2	1.549	1.652
3	2.322	2.477
4	3.096	3.302
5	3.868	4.126
6	4.640	4.949
7	5.410	5.770
8	6.179	6.691
9	6.946	7.409
10	7.712	8.226

Table 4.3: Natural frequencies of Hanger 1 and 2 [Hz]

4.1.2 PE from Bridge Modes

The first 1000 natural frequencies of the Hardanger Bridge were extracted from Abaqus and compared to the ten first frequencies of the two longest hangers, shown in table 4.3. From equation 3.7, with k=1 and for small excitation amplitudes, PE would only occur at twice the natural frequencies of the hangers. Looking at the stability chart in figure 3.6 there is unstable PE for $\frac{\omega_{exc}}{\omega_s}$ = 1.95 and 2.0, and not only 2.0. Frequencies and their mode number of the bridge were therefore extracted with a ratio of 1.95 - 2.05 times the hanger frequencies. The odb.file from Abaqus was used to verify that the bridge modes were in fact vertical modes. The results from these relations can be seen in table 4.4. The table indicate that the ten first mode shapes of the hangers, except for mode ten of Hanger 2, could be excited by the Hardanger Bridge such that PE occur.

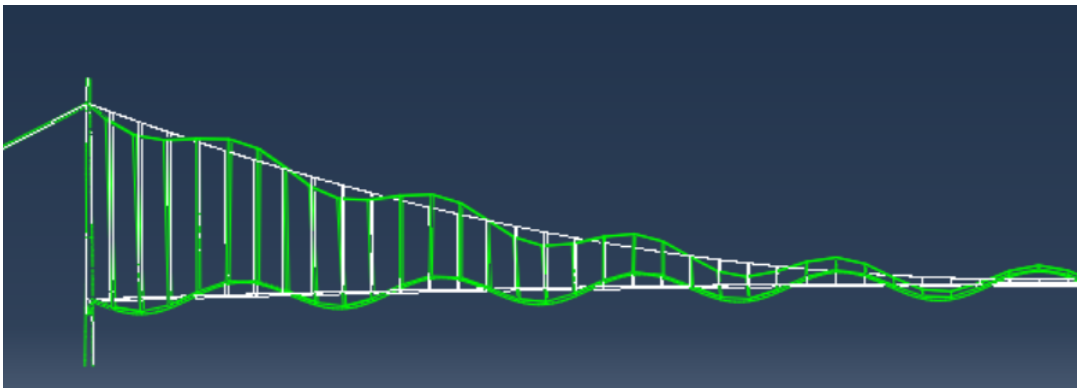

Figure 4.1: Mode 94 of the Hardanger Bridge

Figure 4.1 visualize the 94th mode of the Hardanger Bridge. The mode shape is scaled

with a factor of 20 to accentuate its shape against the original bridge. This is clearly a vertical mode, and if this frequency occur over a certain period of time, this mode could force Hanger 1 into PE. However, it also requires a significant excitation amplitude.

Hanger	Hanger mode	Bridge mode	$\omega_{HB}[Hz]$	$\omega_{HB}/\omega_{Hanger}$
1	1	94	1.564	2.014
1	2	205	3.053	1.965
1	2	209	3.096	1.993
1	2	212	3.143	2.024
1	2	213	3.158	2.033
1	2	214	3.166	2.038
1	3	365	4.666	2.003
1	3	367	4.698	2.017
1	4	427	6.112	1.968
1	5	496	7.604	1.960
1	5	500	7.735	1.993
1	5	508	7.743	1.995
1	6	578	9.264	1.991
1	6	581	9.382	2.016
1	7	602	10.604	1.954
1	7	606	10.899	2.008
1	8	642	12.433	2.006
1	8	646	12.672	2.044
1	9	660	13.617	1.954
1	10	696	15.605	2.017
2	1	100	1.644	1.984
2	1	105	1.695	2.046
2	2	223	3.267	1.972
2	2	238	3.366	2.032
2	3	375	5.029	2.024
2	4	440	6.505	1.964
2	4	452	6.608	1.995
2	5	525	8.126	1.964
2	5	536	8.451	2.042
2	6	588	9.783	1.971
2	6	592	10.137	2.042
2	7	622	11.521	1.990
2	7	624	11.609	2.005
2	8	652	12.971	1.962
2	9	684	14.938	2.010

Table 4.4: Natural frequencies of Hardanger Bridge versus Hanger 1 and 2.

Chapter 5

Fieldwork

5.1 Procedure

After having looked at several theoretical aspects of PE at the Hardanger Bridge, fieldwork at the Hardanger Bridge was executed. The fieldwork was done in March, and was done throughout two days. The first day was used for hammer testing on the two longest hangers and on the bridge girder. Hammer testing was explained in section 2.6. There was also done an hour long recording of ambient vibrations the same day. The next day several more ambient vibration recordings at various locations were executed. Detailed description of each setup can be found in appendix B.

The weather was nice with calm air the first day while doing the hammer tests. See picture 5.1. Thus getting little influence from wind in the input and output measurements. It was more windy the second day, but of no negative influence on the results since this day was spent measuring ambient vibrations. The Hardanger bridge is not a highly trafficked bridge, with a yearly average about 2000 cars/day, so most of the measurements from the hammer tests were done without cars passing over the bridge during recordings.

Figure 5.1: Day 1: Picture of bridge from tower.

5.1.1 Equipment

The main equipment used for the measurements where;

- Large-sledge impact hammer, see figure 5.2a
  - ICP®impact hammer (5.5kg), model 086D50
  - Sensitivity (±15%) = 0.23mV/N
  - Measuring range = ±22240Npk
  - Tip - hard plastic, red, model 084A32

- Three accelerometers, see figure 5.2b
  - Triaxial ICP®accelerometer, model 356$A16$
  - Sensitivity (±10%) = 100mV/g
  - Frequency range (±5%) = 0.5 to 5000Hz
- Dynamic module, see figure 5.2c
  - National Instruments (NI) CompactDAQ
  - NI 9234
- Computer
- Cables
- Lifting platform

Specific sensitivity and range values for utilized sensors can be found in accompanying files, under sub-folder *SensorsDatabase*.

(a) Impact hammer

(b) Accelerometer

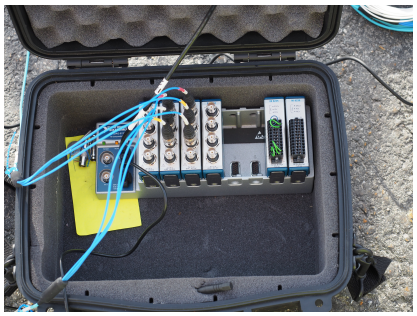

(c) Dynamic module

Figure 5.2: Picture of equipment

5.1.2 Hanger Measurements

Measurements on the two longest hangers were carried out, subsequently called Hanger 1 and Hanger 2. Hanger 1 has a length of 127.53m from pin to pin, and Hanger 2 is 119.75m. To measure the cable response there were used three accelerometers, each measuring acceleration in three directions. One accelerometer was placed on the hanger, one on the girder and one below the connection point. The impact hammer was then successively inflicted on five different locations on the hanger in two directions, rendering ten different inputs and outputs. Global directions were set as demonstrated in figure 5.3.

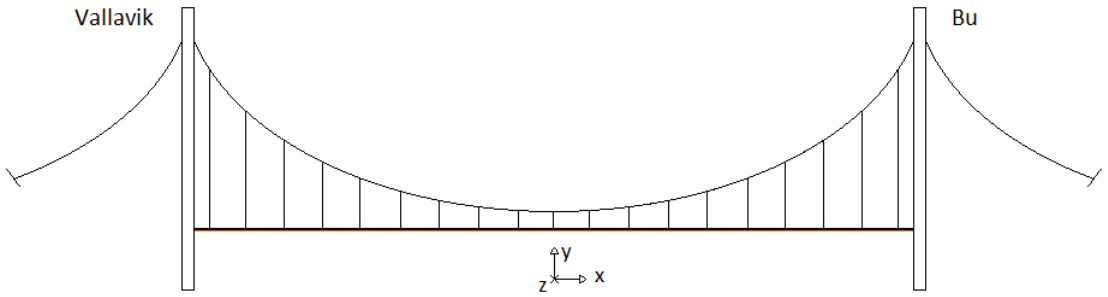

Figure 5.3: Global coordinate directions

Accelerometer 3 was placed on the girder about halfway between the hanger in question and the next hanger. Accelerometer 2 was placed just below where the hanger is connected to the girder. The last one, accelerometer 1 was placed on the hanger, about 12m up from the connection. This was executed using a lifting platform. See figure 5.4 for pictures and table 5.1 for coordinates for each hanger setup. Each hanger has its own local coordinate system, see figure 5.5, where the zero point is located on the girder, directly below the hanger.

The impact hammer's first point of infliction was on the hanger, about 10cm below accelerometer 1. The second point was 2m below the first and subsequently so on for the next points. See table 5.2 for coordinates. For each location the cable was hit from two different directions, x- and z-direction. Each hit from the impact hammer and corresponding response were recorded for 20s. Trying to ensure good enough signals

for later analysis it was important that the impact from the hammer was one single impulse. The power spectral density (PSD) to the input signal was also checked, wanting it to be more or less constant for the desired frequency range, up to $20Hz$. For this range the 20 first natural frequencies were expected to exist within, based on the numerical models. These aspects were checked manually for each hit, and then considering the signal to be adequate, the data from three individual hits at each location were saved.

(a) Accelerometer 1

(b) Accelerometer 2

(c) Accelerometer 3

Figure 5.4: Accelerometer setup on hangers

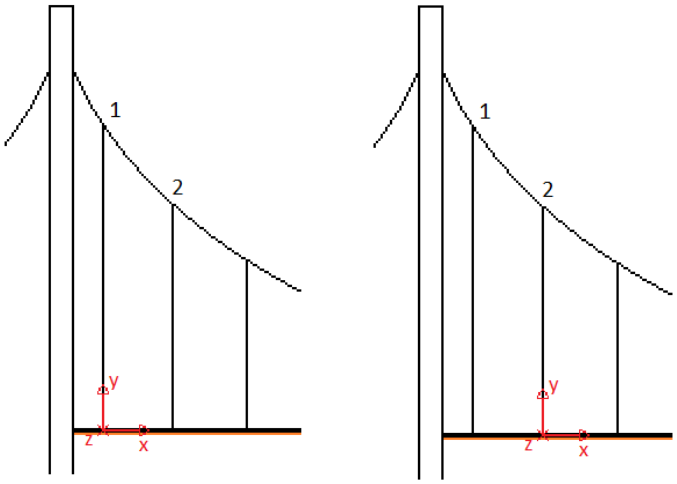

(a) Local zero point Hanger 1 (b) Local zero point Hanger 2

Figure 5.5: Local coordinate systems

	Setup					
Accelerometer	Hanger 1			Hanger 2		
1	0.00	12.50	0.00	0.00	12.35	0.00
2	0.00	0.15	0.00	0.00	0.15	0.00
3	9.54	0.00	0.00	9.60	0.00	0.00
Local coord. [m]	x	y	z	x	y	z

Table 5.1: Coordinates for accelerometers

	Setup					
Hit loc.	Hanger 1			Hanger 2		
1	0.00	12.40	0.00	0.00	12.21	0.00
2	0.00	10.50	0.00	0.00	10.35	0.00
3	0.00	8.50	0.00	0.00	8.35	0.00
4	0.00	6.50	0.00	0.00	6.35	0.00
5	0.00	4.50	0.00	0.00	4.35	0.00
Local coord. [m]	x	y	z	x	y	z

Table 5.2: Coordinates for hit locations on hanger

5.1.3 Girder Measurements

While keeping the accelerometers in the same positions as for the hanger measurements, there were done hammer tests on the girder. For the same accelerometer setup as for Hanger 1, there were done three hits on three different locations along the girder, evenly between accelerometer 2 and 3. Henceforth are these measurements called Girder 1 and measurements with the same setup as for Hanger 2 are called Girder 2. The Girder 1 measurements were recorded for 10s and measurements for Girder 2 were recorded for 20s. See table 5.3 for hit coordinates.

	Setup					
Hit loc.	Girder 1			Girder 2		
1	0.00	0.00	0.00	0.00	0.00	0.00
2	4.42	0.00	0.00	3.50	0.00	0.00
3	9.54	0.00	0.00	6.50	0.00	0.00
4				9.60	0.00	0.00
5				12.40	0.00	0.00
Local coord. [m]	x	y	z	x	y	z

Table 5.3: Coordinates for hit locations on girder

5.1.4 Ambient Vibrations

The measurements for the ambient vibrations were recorded for one hour and measured with five different setups for the three accelerometers. One of the ambient measurement were done with the same setup as for Hanger 1 in the hammer tests, where accelerometer 1 was placed about $12m$ up on the hanger. See table 5.1. The traffic was simultaneously registered to later see if there was any correlation between the recorded vibrations and type of truck. Two other setups were also done on Hanger 1 and 2 the second day. For these measurements accelerometer 3 was placed below the connection point between the hanger and the girder, accelerometer 2 was placed directly on the connection, and accelerometer 1 was placed about $1.5m$ up on the hanger. See table 5.4. As for the hammer tests, there were also done measurements on the girder. For the first girder measurement accelerometer 3 was placed below the connection of Hanger 1, while accelerometer 2 and 1 was spread evenly out over about 9m towards the pylon. Another similar girder measurement where done for Hanger 2. Accelerometer 3 now placed below the connection point on Hanger 2, and the other two spread evenly out over about $12m$ towards Hanger 1. These setups are henceforth called Girder 0 and Girder 1, respectively. See coordinates for the accelerometers in table 5.5, with local zero point as for Hanger 1 and 2 in the hammer tests.

	Ambient setup					
Accelerometer	Hanger 1			Hanger 2		
1	0.00	1.70	0.00	0.00	1.65	0.00
2	0.00	0.55	0.00	0.00	0.56	0.00
3	0.00	0.15	0.00	0.00	0.20	0.00
Local coord. $[m]$	x	y	z	x	y	z

Table 5.4: Coordinates for accelerometers for ambient measurement on hangers

	Ambient setup					
Accelerometer	Girder 0			Girder 1		
1	-8.56	0.00	0.00	-12.60	0.00	0.00
2	-4.57	0.00	0.00	-6.60	0.00	0.00
3	0.00	0.15	0.00	0.00	0.20	0.00
Local coord. $[m]$	x	y	z	x	y	z

Table 5.5: Coordinates for accelerometers for ambient measurements on girder

5.2 Results

5.2.1 Processing of Signals

Accelerometers were setup in the global coordinate directions for all accelerometers, except for the accelerometer placed on the hanger. The accelerometer on the hanger was mounted on an open steel cylinder, which again was mounted to the hanger on locations given in table 5.1 and 5.4. The open cylinder had a thin inner layer of rubber to prevent any damages on the hangers. This also helped the cylinder to stay in place during the experiment without to much pressure on the cable, see figure 5.7.

The signals from the accelerometer on the hanger needed to be decomposed in global directions before further analysis could proceed. The angle between the local coordinates on the accelerometer on the hanger and the global directions were found by searching for minimum energy in global y-direction. The minimum energy is proportional to the square of acceleration, hence the acceleration vectors were summed and squared. This gave an angle of 41.2 °.

Figure 5.6: Accelerometer mounted to steel section

Figure 5.7: Installation of accelerometer on hanger 1

5.2.2 Results from Modal Analysis Methods

A MATLAB toolbox for experimental modal analysis, called EasyMod, and supplemented scripts developed by Postdoc Daniel Cantero were used to analyse the measurements. This toolbox uses three identification methods. Two of the methods are SISO methods and one is a MIMO method. They are respectively, CF and LF, and LSCE, explained in section 2.7.

These methods could be used to estimate natural frequencies, mode shapes and damping ratios. The toolbox also provides some validation of the results, in form of mode shape comparison and modal collinearity for a comparison of two sets of analysis. After having inputted various data into the script, it was seen that the natural frequencies could be estimated fairly well, but damping was hard to estimate. The mode shapes could be visualized adequately, but were highly dependent on the locations of the sensors. This will be discussed more in section 5.2.3.

The signals inputted were zero-padded before processing, meaning that the time-domain signal was added zeros at the start and end of the signal. Choosing a zero padding of five times the original signal, the new signal was 11 times longer than the original. Thus resulting in a more refined frequency domain signal, see section 2.3.2. As the scripts

only process signals in one direction at a time, the methods were executed on input and output for the same direction.

Having processed several various signals, experience indicated that the LSCE method gave very uneven results. The method was highly dependent on how many modes considered in the analysis, especially for the measured signals but not limited to. The error curve was without any noticeable drops indicating the correct number of modes. For more on LSCE see section 2.7.3. The results from LSCE were therefore not retrieved, and are not presented in this thesis.

For the other two methods, CF and LF, it was executed a manual selection for one or more frequency ranges from a summed FRF. Picking the range around each pronounced peak, see figure 5.8. The summed FRF is a sum of the mean FRFs calculated for the three hits at each location. The methods then calculated the natural frequency and damping ratio for one mode within the chosen frequency range. For the selected modes, CF and LF calculate one estimate for each hit location, choosing the estimate with best approximation. The estimates for damping were highly dependent on how these frequency ranges were chosen, so the results varied from one analysis to the next, and were therefore not retrieved. The natural frequencies seldom varied more than per thousand, and are presented in tables tables 5.6 to 5.9. As informed, the toolbox picks out the frequency with the best approximation to the estimated FRF for each mode. Presented in the tables are also the mean value with the standard deviation considering the estimated frequencies at all hit locations, in this case five locations.

The first five natural frequencies were the ones that gave the clearest peak, except for the lowest frequency. This was especially a problem for the fundamental frequencies in x-direction, where the peaks were undefined. Based on this and the likelihood that higher modes would be suppressed by damping, natural frequencies up to the tenth mode were extracted. Even though the connections to the girder and main cable should be pinned in x-and z-directions, it was noticed a variation in natural frequencies. The frequencies in z-direction tended to be lower than in x-direction. Pursuant to

Mersenne's law, see section 2.5, the natural frequencies should be linear as a function of mode number, with the slope dependent on the effective length, density and tension. Since the density and tension are constant for the cable, this deviation in frequencies has to be owing to the fact that the connection is not perfectly pinned in all directions. Thus, the hangers seem to have different effective lengths in different directions.

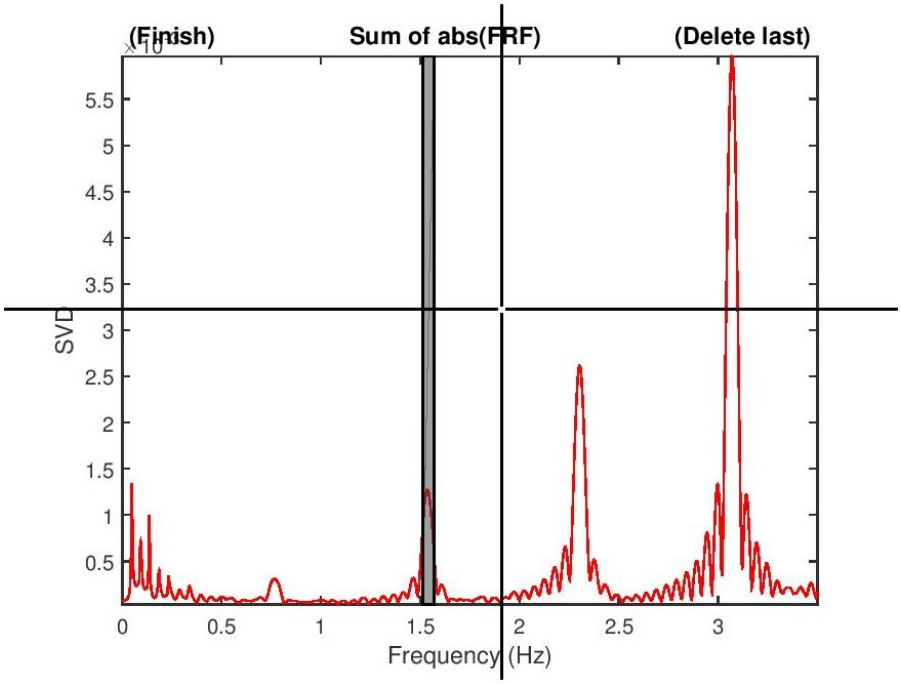

Figure 5.8: Interactive window for selecting of frequency ranges

Circle Fit

In table 5.6 and 5.7, respectively Hanger 1 and Hanger 2, the first ten natural frequencies estimated with CF are presented. The emphasized frequencies are the best approximation, and the mean value and the standard deviation are calculated from the estimates at each location. These frequencies are listed in appendix A. Both x- and z-direction are presented, clearly showing a lower frequency in z-direction, except for the fundamental frequency.

	Hanger 1					
Mode	*x-dir*	μ	σ	*z-dir*	μ	σ
1	*0.776*	0.760	0.0096	*0.778*	0.772	0.0143
2	*1.552*	1.538	0.0079	*1.538*	1.536	0.0022
3	*2.317*	2.325	0.0055	*2.297*	2.304	0.0051
4	*3.101*	3.094	0.0040	*3.076*	3.072	0.0049
5	*3.874*	3.869	0.0043	*3.841*	3.842	0.0021
6	*4.653*	4.647	0.0048	*4.643*	4.640	0.0033
7	*5.433*	5.427	0.0063	*5.377*	5.377	0.0044
8	*6.204*	6.206	0.0061	*6.164*	6.156	0.0046
9	*6.999*	6.991	0.0066	*6.985*	6.983	0.0017
10	*7.782*	7.775	0.0060	*7.804*	7.788	0.0097

Table 5.6: Natural frequencies extracted with CF method from hanger 1, with mean and standard deviation.

	Hanger 2					
Mode	*x-dir*	μ	σ	*z-dir*	μ	σ
1	*0.789*	0.787	0.0198	*0.777*	0.777	0.0105
2	*1.584*	1.586	0.0048	*1.581*	1.575	0.0048
3	*2.375*	2.373	0.0038	*2.360*	2.361	0.0056
4	*3.163*	3.164	0.0019	*3.153*	3.148	0.0084
5	*3.959*	3.957	0.0020	*3.942*	3.932	0.0055
6	*4.756*	4.755	0.0034	*4.707*	4.705	0.0050
7	*5.555*	5.552	0.0016	*5.639*	5.630	0.0080
8	*6.352*	6.352	0.0034	*6.418*	6.415	0.0028
9	*7.157*	7.157	0.0012	*7.215*	7.213	0.0108
10	*7.960*	7.959	0.0024	*7.958*	7.957	0.0020

Table 5.7: Natural frequencies extracted with CF method from hanger 2, with mean and standard deviation.

Line Fit

In table 5.8 and 5.9, respectively Hanger 1 and Hanger 2, the first ten natural frequencies estimated with LF are presented. As for CF, the tables lists the best approximation, the mean value and the standard deviation. Both axis are also presented here. A lower frequency in z-direction applies still, and for Hanger 2 also for the fundamental frequency.

	Hanger 1					
Mode	*x-dir*	μ	σ	*z-dir*	μ	σ
1	*0.757*	0.756	0.0174	*0.765*	0.770	0.0042
2	*1.545*	1.543	0.0019	*1.540*	1.540	0.0035
3	*2.323*	2.321	0.0010	*2.301*	2.303	0.0020
4	*3.092*	3.094	0.0014	*3.077*	3.073	0.0023
5	*3.870*	3.871	0.0011	*3.842*	3.845	0.0018
6	*4.647*	4.647	0.0014	*4.648*	4.645	0.0014
7	*5.427*	5.427	0.0019	*5.377*	5.378	0.0011
8	*6.207*	6.207	0.0017	*6.160*	6.162	0.0015
9	*6.993*	6.994	0.0019	*6.988*	6.989	0.0012
10	*7.776*	7.777	0.0018	*7.799*	7.791	0.0056

Table 5.8: Natural frequencies extracted with LF method from hanger 1, with mean and standard deviation.

	Hanger 2					
Mode	*x-dir*	μ	σ	*z-dir*	μ	σ
1	*0.795*	0.796	0.0141	*0.776*	0.779	0.0039
2	*1.583*	1.584	0.0009	*1.574*	1.573	0.0009
3	*2.375*	2.373	0.0008	*2.361*	2.360	0.0009
4	*3.162*	3.167	0.0023	*3.147*	3.148	0.0016
5	*3.961*	3.958	0.0013	*3.938*	3.933	0.0032
6	*4.756*	4.757	0.0006	*4.712*	4.709	0.0018
7	*5.554*	5.555	0.0006	*5.637*	5.629	0.0046
8	*6.354*	6.356	0.0008	*6.416*	6.418	0.0015
9	*7.156*	7.159	0.0018	*7.215*	7.216	0.0050
10	*7.965*	7.963	0.0027	*7.962*	7.961	0.0007

Table 5.9: Natural frequencies extracted with LF method from hanger 2, with mean and standard deviation.

5.2.3 Validation of MATLAB Software

The toolbox was tested to acquire information of where it would be suitable to place sensors on the hanger to extract reliable results. Two tests were executed, where different node sets were placed on various hanger locations, simulating accelerometers. All tests were executed in Abaqus, with one simulated hit. Hangers were modelled as presented in section 4.1.1. Accelerations at desired nodes were extracted from Abaqus and used as input to the toolbox.

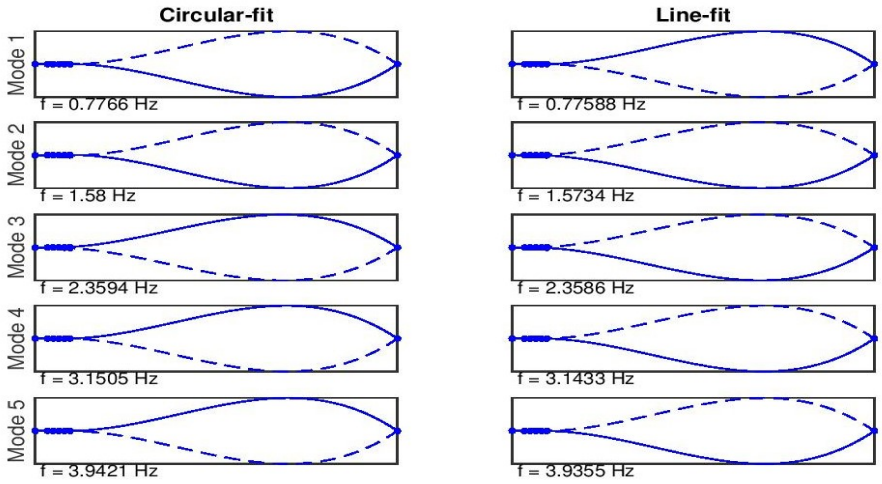

Figure 5.9: Natural frequencies and mode shapes of Hanger 2 in z-direction.

The accelerations from the Hardanger Bridge were implemented in the toolbox and the mode shapes from CF and LF were extracted. Mode shapes were difficult to extract because of the high concentration of hits at the lower hanger end. Figure 5.9 visualize the first five natural frequencies with the respective mode shapes of Hanger 2 at the Hardanger Bridge. There were no hits above $12m$ and therefore no point to interpolate between $12m$ and hanger end. The toolbox is sensitive to noise, and that could be one of the reasons for those poor mode shape results. Z-direction gave clearer response in the FRF, and is therefore used to compare mode shapes and natural frequencies in this section.

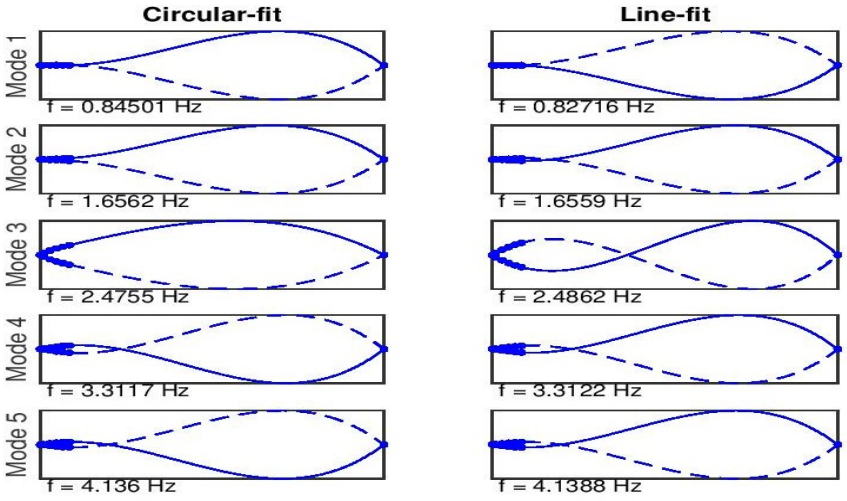

Figure 5.10: Natural frequencies and mode shapes of Hanger 2 with 5 nodes.

Figure 5.10 shows the frequencies and the mode shapes from the first hammer test simulation in Abaqus. This test was performed similar to the actual test to validate the real tests and the EasyMod toolbox. The coordinate direction of where to hit is irrelevant in Abaqus, since the cross section is symmetric and perfectly pinned in all directions. The simulated signals were added noise with a signal to noise ratio of 60. Compared to the frequencies given in table 4.3 the toolbox in MATLAB gave quite accurate results. With a lower signal to noise ratio there was a problem to extract results for the two first natural frequencies. Despite the close accuracy of the natural frequencies, the mode shapes were not computed correctly.

An analysis in Abaqus with output from nine nodes evenly distributed over the length was carried out. These signals were also added a signal to noise ratio of 60 before inputed in the MATALB toolbox. The results became more accurate with respect to the mode shapes. Figure 5.11 shows the five first natural frequencies and their respective mode shapes.

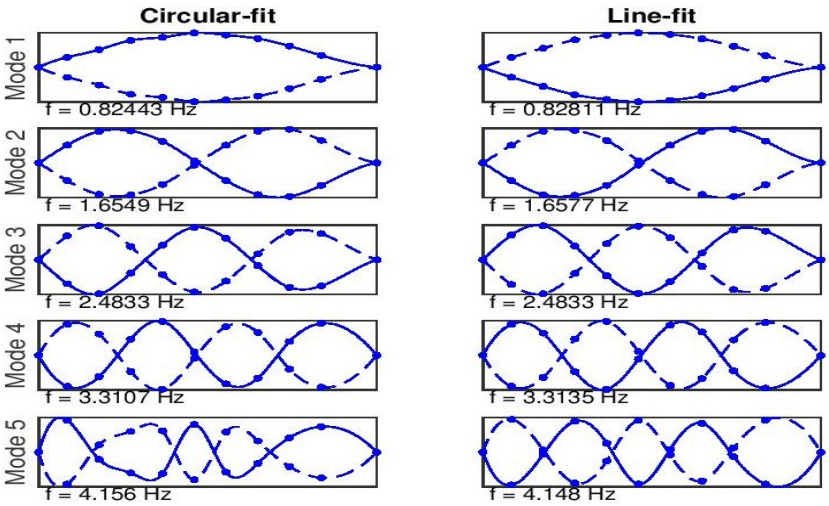

Figure 5.11: Natural frequencies and mode shapes of Hanger 2 with 9 nodes.

There were done several attempts on extracting the damping ratios from the analysis. The damping was set as Rayleigh damping in the Abaqus input file, and the expected damping ratios from the MATLAB software were anticipated to have higher damping

ratios for higher modes. However, the results showed a decrease in damping ratio for higher natural frequencies. The tests presented above were also done without any noise to see if the damping changed with perfect signals. But the damping ratios did not correlate between tests, other than decreasing for higher modes. On basis of this, damping has not been investigated further for the measurements.

5.3 Validation of Numerical Model

The numerical model was based on the technical drawings and steel properties. Validation of the numerical model was done by comparing the extracted frequencies to the estimated natural frequencies from the hammer tests. For the estimated values the frequencies with best approximation to the estimated FRF were chosen for the comparison. The frequencies were relatively similar for Hanger 1, but the frequencies for Hanger 2 were noticeable dissimilar. Mersenne's law, see section 2.5, was utilized to calculate length and tension to corresponding frequencies. These values were then compared against assumed values from technical drawings, presented in table 4.2. Mersenne's law do not include non-linearity, and thus some margin of error to the calculations can be seen.

Assuming the measured tension retrieved from the technical drawings to be applicable to the estimations, the corresponding length to each estimated frequency was calculated. For Hanger 1 the lengths are presented in table 5.10 and for Hanger 2 in table 5.11. The lengths were calculated for frequencies estimated in both x- and z-direction, and subsequently for CF and LF. Studying the values, it was evident that the frequencies for x-direction have corresponding shorter lengths, indicating a stiffer joint than the design or at least not equally pinned in all directions. This difference is more prominent for Hanger 1 than Hanger 2. The lengths calculated for Hanger 1 are close to the actual length of the hanger, pin to pin. However, for Hanger 2, the lengths are significantly higher than the actual length. Indicating that the tension in the hanger is not as assumed.

	Hanger 1 - Length [m]			
	x-direction		z-direction	
Mode	CF	LF	CF	LF
1	127.22	130.39	130.39	129.07
2	127.27	127.87	127.87	128.23
3	127.85	127.52	127.52	128.78
4	127.39	127.75	127.75	128.39
5	127.48	127.59	127.59	128.53
6	127.34	127.50	127.50	127.50
7	127.25	127.39	127.39	128.57
8	127.34	127.28	127.28	128.26
9	127.00	127.10	127.10	127.18
10	126.91	127.01	127.01	126.63
Mean value:	127.30	127.74	127.74	128.12

Table 5.10: Hanger 1: Calculated length of cable for estimated frequency

	Hanger 2 - Length [m]			
	x-direction		z-direction	
Mode	CF	LF	CF	LF
1	125.29	124.42	127.36	127.48
2	124.91	124.94	125.11	125.67
3	124.92	124.96	125.74	125.69
4	125.09	125.12	125.50	125.71
5	124.91	124.85	125.47	125.59
6	124.78	124.77	126.07	125.95
7	124.64	124.66	122.79	122.82
8	124.57	124.53	123.29	123.33
9	124.38	124.40	123.37	123.37
10	124.26	124.19	124.28	124.23
Mean value:	*124.77*	*124.69*	*124.90*	*124.98*

Table 5.11: Hanger 2: Calculated length of cable for estimated frequency

When calculating the tension in the hangers for corresponding frequencies, assuming the lengths to be as designed, the accuracy of the assumed tension could be assessed. Examining first the results for Hanger 1, in table 5.12, the tension calculated do not deviate significantly from the assumed tension. However, the values for z-direction are somewhat lower. Seeing as the calculated lengths in z-directions were tending to

a higher value, it is possible that the actual tension is closer to the mean tension calculated for z-direction. This because the effective length is limited by the connections and could only be shorter due to a stiffer joint.

	Hanger 1 - Tension [N]			
	x-direction		z-direction	
Mode	CF	LF	CF	LF
1	985	937	990	957
2	984	975	967	969
3	975	980	958	961
4	982	977	966	967
5	981	979	964	965
6	983	980	979	981
7	984	982	964	964
8	983	984	970	969
9	988	987	984	985
10	990	988	995	994
Mean value:	983	977	974	971

Table 5.12: Hanger 1: Calculated tension in cable for estimated frequency

Assessing the calculated tensions for estimated frequencies on Hanger 2, the tensions clearly deviates from the assumed tension. Instead of a tension close to $1000kN$, the tensions calculated are barely above $900kN$. As these are lower values than the assumed value it is not necessarly a concern for the bridge, but it is significant to the numerical model.

To demonstrate the deviation of the estimated natural frequencies from the natural frequencies extracted from Abaqus, the difference is presented in table 5.15 and 5.16, respectively Hanger 1 and Hanger 2. The mean deviations of all ten modes are stated at the bottom of the tables. The extracted frequencies the estimates were compared against are presented in table 5.14. The original frequencies are natural frequencies with tension as retrieved from the technical drawings, while the adjusted frequencies are altered adapting the mean tension calculated from all estimated natural frequencies, respectively $976kN$ and $905kN$ for Hanger 1 and Hanger 2.

	Hanger 2 - Tension [N]			
	x-direction		z-direction	
Mode	CF	LF	CF	LF
1	898	911	869	867
2	903	903	901	893
3	903	903	892	892
4	901	900	895	892
5	903	904	895	894
6	905	905	887	889
7	907	907	935	934
8	908	909	927	927
9	911	911	926	926
10	913	914	913	913
Mean value:	*905*	*907*	*904*	*903*

Table 5.13: Hanger 2: Calculated tension in cable for estimated frequency

In table 5.15 the mean deviations are less than one percent, indicating that the numerical model for Hanger 1 is a good estimate for the actual hanger. The adjusted model do not alter the result considerably. Studying table 5.16 for Hanger 2, the deviations are significantly higher for the original numerical model. However, the adjusted model decreases the deviation vastly. Other alterations were also examined, but without any significant improvement. A possible improvement could have been to model two different hangers for x- and z-direction as the frequencies indicate some variation in effective length, but seeing as the difference is small, one model was adopted.

	Hanger 1		Hanger 2	
Mode	original	adjusted	original	adjusted
1	0.774	0.773	0.826	0.792
2	1.549	1.545	1.652	1.585
3	2.322	2.318	2.477	2.377
4	3.096	3.089	3.302	3.168
5	3.868	3.860	4.126	3.959
6	4.640	4.630	4.949	4.748
7	5.410	5.399	5.770	5.537
8	6.179	6.166	6.591	6.324
9	6.946	6.932	7.409	7.109
10	7.712	7.697	8.226	7.893

Table 5.14: Generated natural frequencies from Abaqus

	Hanger 1							
	x-direction				z-direction			
	original		adjusted		original		adjusted	
Mode	CF	LF	CF	LF	CF	LF	CF	LF
1	0.3 %	2.2 %	0.5 %	2.0 %	0.5 %	1.2 %	0.7 %	1.0 %
2	0.2 %	0.2 %	0.4 %	0.0 %	0.7 %	0.5 %	0.5 %	0.3 %
3	0.2 %	0.1 %	0.0 %	0.2 %	1.1 %	0.9 %	0.9 %	0.7 %
4	0.2 %	0.1 %	0.4 %	0.1 %	0.6 %	0.6 %	0.4 %	0.4 %
5	0.1 %	0.1 %	0.3 %	0.3 %	0.7 %	0.7 %	0.5 %	0.5 %
6	0.3 %	0.2 %	0.5 %	0.4 %	0.1 %	0.2 %	0.3 %	0.4 %
7	0.4 %	0.3 %	0.6 %	0.5 %	0.6 %	0.6 %	0.4 %	0.4 %
8	0.4 %	0.5 %	0.6 %	0.7 %	0.2 %	0.3 %	0.0 %	0.1 %
9	0.7 %	0.7 %	1.0 %	0.9 %	0.6 %	0.6 %	0.8 %	0.8 %
10	0.9 %	0.8 %	1.1 %	1.0 %	1.2 %	1.1 %	1.4 %	1.3 %
Mean value:	*0.4 %*	*0.5 %*	*0.5 %*	*0.6 %*	*0.6 %*	*0.7 %*	*0.6 %*	*0.6 %*

Table 5.15: Deviation from numerical models for Hanger 1

	Hanger 2							
	x-direction				z-direction			
	original		adjusted		original		adjusted	
Mode	CF	LF	CF	LF	CF	LF	CF	LF
1	4.4 %	3.7 %	0.4 %	0.3 %	6.0 %	6.1 %	2.0 %	2.1 %
2	4.1 %	4.1 %	0.1 %	0.1 %	4.3 %	4.7 %	0.2 %	0.7 %
3	4.1 %	4.1 %	0.1 %	0.1 %	4.7 %	4.7 %	0.7 %	0.7 %
4	4.2 %	4.2 %	0.2 %	0.2 %	4.5 %	4.7 %	0.5 %	0.7 %
5	4.0 %	4.0 %	0.0 %	0.1 %	4.5 %	4.6 %	0.4 %	0.5 %
6	3.9 %	3.9 %	0.2 %	0.2 %	4.9 %	4.8 %	0.9 %	0.8 %
7	3.7 %	3.8 %	0.3 %	0.3 %	2.3 %	2.3 %	1.8 %	1.8 %
8	3.6 %	3.6 %	0.4 %	0.5 %	2.6 %	2.6 %	1.5 %	1.5 %
9	3.4 %	3.4 %	0.7 %	0.7 %	2.6 %	2.6 %	1.5 %	1.5 %
10	3.2 %	3.2 %	0.8 %	0.9 %	3.2 %	3.2 %	0.8 %	0.9 %
Mean value:	*3.9 %*	*3.8 %*	*0.3 %*	*0.3 %*	*4.0 %*	*4.0 %*	*1.0 %*	*1.1 %*

Table 5.16: Deviation from numerical models for Hanger 2

5.4 Possible Reasons for Vibration

The development of PE reported on previous bridges were presented in the introduction. Both traffic and wind induced vibrations were proposed to have an influence on the excitations. The traffic on the Hardanger Bridge was retrieved and analyzed together with ambient vibration tests. High frequent vibrations were observed on site,

even without any cars passing. The wind data, from the same time interval, were therefore analyzed in a search to find a correlation to the vibrations.

5.4.1 Traffic

Figure 5.12 shows the accelerations for the ambient setup on day one, see section 5.1.4. Figure 5.12a visualize the accelerations in x-direction, and figure 5.12b visualize the accelerations in z-direction, both from accelerometer 1 on Hanger 1. Figure 5.12c visualize the accelerations in y-direction from accelerometer 2 below the connection of Hanger 1. Pictures of passing traffic were taken to check their influence on the accelerations on the bridge. The pictures were taken at the moment of entering or leaving the bridge at the Vallavik side. The time stamps for the pictures were saved to accurately place them on the time line together with the ambient vibration data. The green circles in figure 5.12 indicate a car and the red crosses indicate trucks passing the accelerometers. Peaks in the acceleration plot can be seen when a truck has passed, but the accelerations seem to decay before any further excitation occur. Accelerations in z-direction are generally lower than for x-direction, and this might be due to the direction of the traffic or the direction of the wind. The influence from cars were not very significant. A prominent peak around $600s$ into the recording can be seen without any entered traffic. This is probably due to the inconsistent capturing of passing cars, and is most likely due to a truck.

Looking closer at the time interval around $1900s$ into the accelerations, figure 5.13 shows a clear peak in the accelerations. It is most likely induced by the truck displayed in red. If it was PE the accelerations should increase exponentially, like the displacements in figure 3.2a in section 3.2.1. Instead the accelerations decay over the next $15s$. This is also the case for the other acceleration peaks in figure 5.12. From the Abaqus simulations of PE the accelerations were much higher than what was the case in these situations.

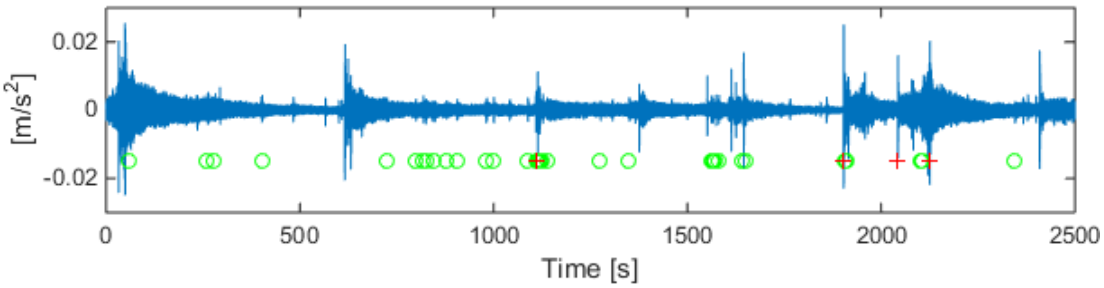

(a) Accelerations in x-direction on Hanger 1.

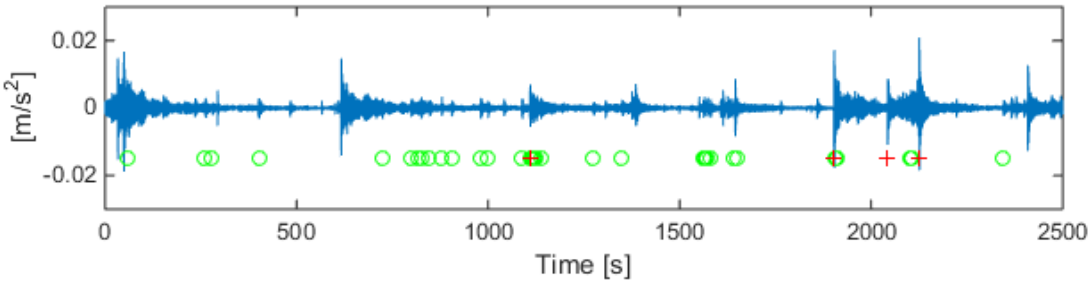

(b) Accelerations in y-direction on joint.

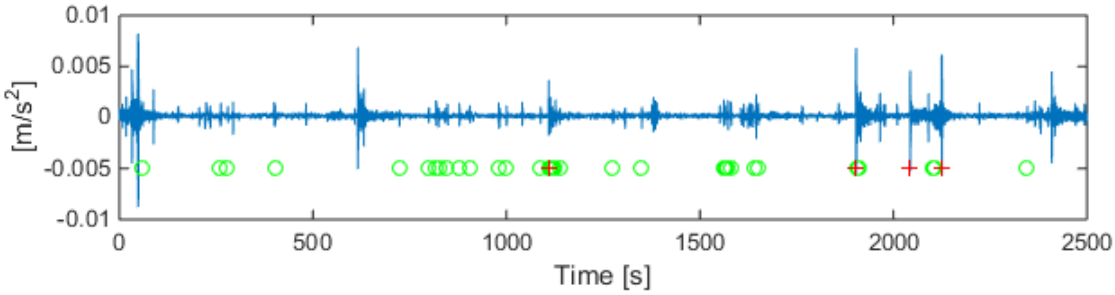

(c) Accelerations in z-direction on Hanger 1.

Figure 5.12: Accelerations and traffic from Hanger 1 and right below.

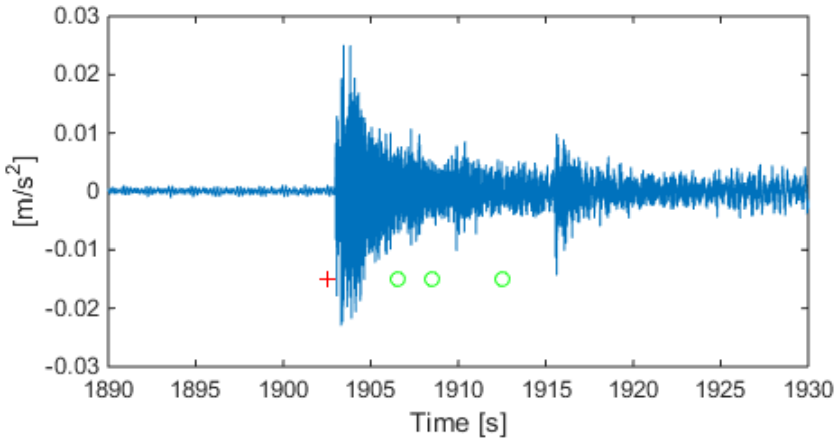

Figure 5.13: Detail of figure 5.12a.

5.4.2 Wind

The vibrations detected on the Hardanger Bridge could also be due to vortex shedding. Simple analysis on the ambient vibration tests from day two indicate that this could be the case. Presented in figure 5.14 are the recorded wind velocities from an accelerometer placed on Hanger 12. From formulas on vortex shedding, presented in section 2.8, the shedding frequencies with these wind velocities would be in a range from $16Hz$ to $32Hz$, assuming $S_t = 0.19$.

Assuming the wind velocities recorded at Hanger 12 to be correlated with the wind velocities at Hanger 2, the ambient recordings on Hanger 2 was analyzed and compared. In figure 5.15 the spectrogram of the signal is plotted, showing the exited frequencies varying over time. Studying the spectrum it is clear that the frequencies excited match the anticipated shedding frequencies. The distribution of excited frequencies during the time step is presented in the (PSD) plot in figure 5.16, where the prominent frequencies are within $16Hz$ and $32Hz$. Based on the estimates from section 5.2.2, the natural frequencies of Hanger 2 would exist with an interval of approximately $0.8Hz$, which coincides with the excited frequencies in the PSD plot.

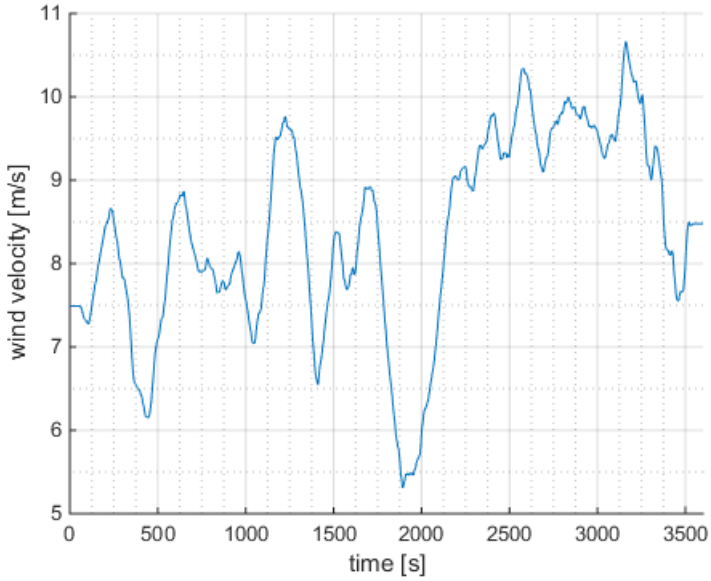

Figure 5.14: Wind velocities recorded on Hanger 12 simultaneously as ambient vibrations on Hanger 2

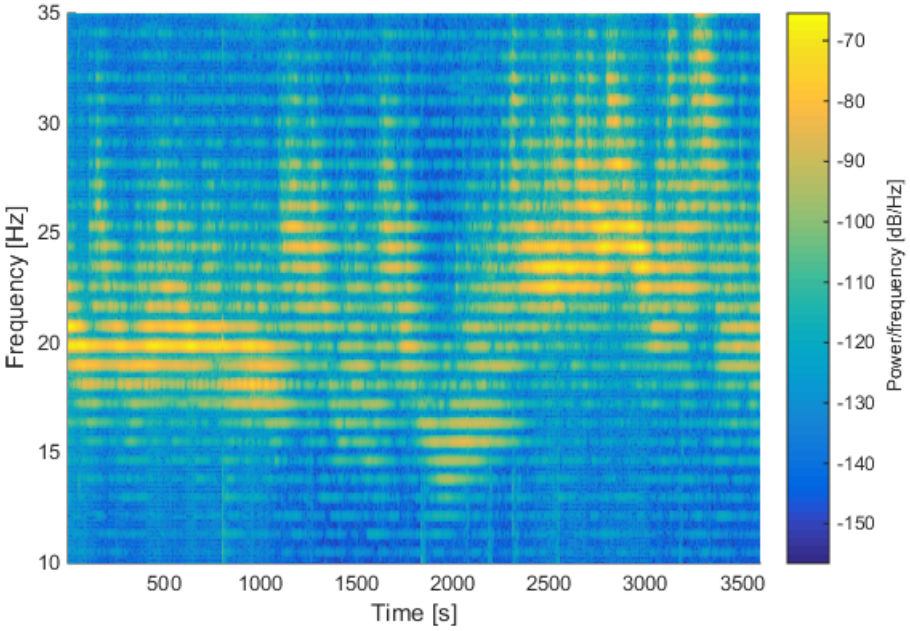

Figure 5.15: Spectrogram of ambient measurements on Hanger 2

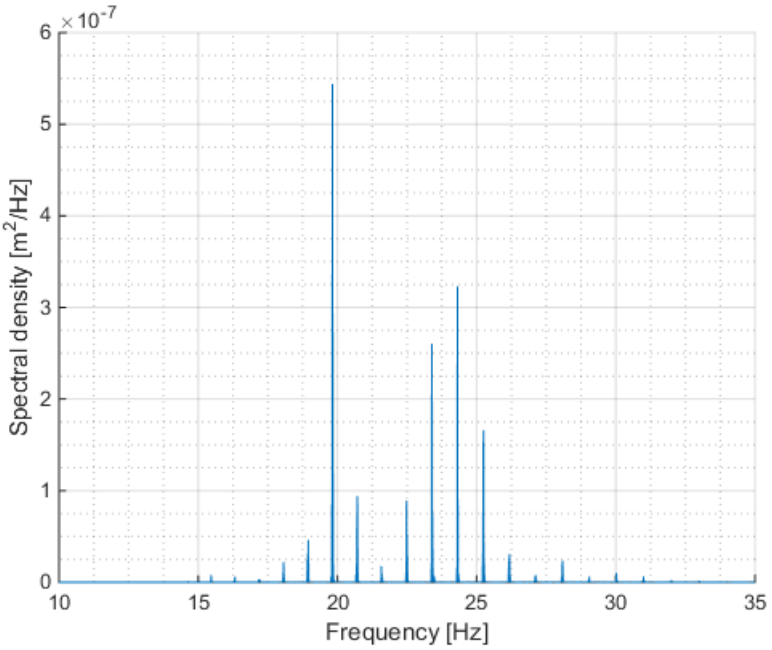

Figure 5.16: PSD plot

Chapter 6

Discussion and Conclusions

6.1 Parametric Excitation

Based on the results from the modal analyses being reliable and relatively in accordance with the actual natural frequencies, PE would occur if the hangers were excited by a frequency close to twice the frequency of one of the natural frequencies estimated. PE other than at twice the frequency is possible, but needs a larger excitation amplitude to initiate. The hangers could possibly be excited by the bridge modes or by traffic.

Seeing as the bridge modes are such low for a suspension bridge of this size, the likelihood of PE because of bridge modes is very improbable. However, if this was the case, the bridge modes likely to excite at twice the natural frequency are very high modes. Even if these frequencies are actual vertical modes and affecting the girder, it is even less likely that these modes would induce the required amplitude to induce PE. This is already an issue when exciting the lowest frequencies of the hangers, so the higher modes would need even higher bridge modes. When looking at the onset of PE, pointed out in section 3.3.3, the lowest modes, in contrast to the higher modes, are excited for a noticeable longer period before the vibrations starts to increase exponentially. Thus, decreasing the likelihood of PE because of bridge modes even more.

This period of excitation before onset of PE would also be an issue when investigat-

ing traffic as cause of PE. While exploring this possibility closer some limitations were clear, smaller cars alone would not likely cause significant vertical displacement of the deck, the focus was therefore on bigger vehicles like trucks and busses. However, as mentioned previously, even with a significant amplitude, the period before onset of PE is from experience relatively long except for fairly high amplitudes.

Previous experience of PE from other bridges are mostly recorded for cable-stayed bridges, not suspension bridges. Reason for more frequently PE on cable-stayed bridges could be that the stay-cables can be excited of both girder and pylon vibrations. However, also here is the required amplitudes of the girder or tower oscillations relatively large, so the phenomenon happens to be rare. In *Cable Vibrations in Cable-Stayed Bridges* [5], there is presented a table listing threshold amplitudes of oscillation for PE at twice the frequency. Where it can be concluded that PE is not unfeasible for small damping ratios. However, it is also pointed out the same requirement as discussed earlier in this section, that PE requires persistence of oscillations for a certain period before onset.

6.2 Evaluation of Consequences

Concluding that the vibrations detected on the Hardanger Bridge are not due to PE, but rather possibly due to vortex shedding, other experiments should be executed. PE can cause quite large displacements from a relatively small initiated movement and create large oscillation in tension. While vibrations induced by vortex shedding are self-limiting, meaning that the effect decreases when the fluctuating structural vibrations become large [16].

Vortex shedding is a well-known phenomenon on bridges, and in case of resonance, when the shedding frequency is equivalent to the natural frequencies, quite harmful vibrations can occur. Though, even without resonance, these varying forces should not be ignored considering the possible long term fatigue effect [17]. If the vibrations continues to be a problem, there are measures to utilize to stabilize the hangers. Cable

to cable connections or installations of oil dampers to mention some [13]. Though, seeing as this thesis main aim was to verify if the vibrations were due to PE, vortex shedding as a possibility has only been looked at briefly and the consequences has not been investigated thoroughly.

6.3 Further Work

After both validating the EasyMod toolbox and comparing the estimated results with numerical models, the natural frequencies from CF and LF seem to produce relatively good estimates. However, there are some improvements to consider, like:

- location of sensors
- weather conditions
- traffic

Locating the sensors more evenly over the length in test simulations, see 5.3, gave good estimates for the mode shapes up to the mode equivalent to the number of sensor locations. Some interfering from noise is also likely, seeing as some frequencies were harder to estimate, especially the fundamental frequency. This coincided with the test simulations, where adding noise to the signal first influenced the estimate of the two lowest frequencies. Considering that the wind was quite calm while the hammer tests were executed the influence from wind was scarce. However, the influence from traffic could have been avoided more consistently during recording of the signals.

Because the methods utilized in this thesis produced undependable damping estimates, no results with suggestions to damping ratios were presented. The modal analyses used to estimate damping ratios in this thesis were all input-output methods and the utilization of output-only methods could possible provide more reliable results if this had been looked into.

This thesis main aim was to verify if PE was the reason for the detected vibrations at

The Hardanger Bridge. As PE was dismissed, the cause of the vibrations are yet to be confirmed. Proposition for further investigation:

- vortex shedding

Vortex shedding as cause have been mentioned in this thesis and are considered feasible. The possible long term fatigue on the hangers from the vibrations should not be disregarded, and further investigation should be carried out.

References

[1] AGK (2008). 12-2950 hardangerbrua beregninger kapittel 1: Grunnlag. Report, Norwegian Public Roads Administration.

[2] Bouten, C. V., Koekkoek, K., Verduin, M., Kodde, R., and Janssen, J. D. (1997). A triaxial accelerometer and portable data processing unit for the assessment of daily physical activity. *Biomedical Engineering, IEEE Transactions on*, 44(3):136–147.

[3] Cantero, D., Rønnquist, A., and Næss, A. (2016). Parametric excitation of mooring cables for submerged floating tunnels. *IABSE Guangzhou 2016*.

[4] de Normalisation, C. E. (1992). *Eurocode 3: Design of Steel Structures: Part 1-1: General Rules and Rules for Buildings*. European Committee for Standardization.

[5] de Sá Caetano, E. (2007). *Cable vibrations in cable-stayed bridges*, volume 9. IABSE.

[6] Fu, Z.-F. and He, J. (2001). *Modal analysis*. Butterworth-Heinemann.

[7] Gadella, M., Giacomini, H., and Lara, L. (2015). Periodic analytic approximate solutions for the mathieu equation. *Applied Mathematics and Computation*, 271:436–445.

[8] Irvine, H. M. and Irvine, M. (1992). *Cable structures*. Number Sirsi) i9780486671277.

[9] Labonnote, N. (2012). *Modal hammer for dummies*.

[10] Larsen, P. K. (1990). *Dimensjonering av stålkonstruksjoner*. Tapir.

[11] Lilien, J.-L. and Da Costa, A. P. (1994). Vibration amplitudes caused by parametric excitation of cable stayed structures. *Journal of Sound and Vibration*, 174(1):69–90.

[12] Maia, N. M. M. and e Silva, J. M. M. (1997). *Theoretical and experimental modal analysis*. Research Studies Press Taunton.

[13] Matsumoto, M., Shiraishi, N., and Shirato, H. (1992). Rain-wind induced vibration of cables of cable-stayed bridges. *Journal of wind engineering and industrial aerodynamics*, 43(1):2011–2022.

[14] Nayfeh, A. H. and Mook, D. T. (2008). *Nonlinear oscillations*. John Wiley & Sons.

[15] Schiller, K. (1973). Change of frequency with temperature in stringed musical instruments. *Journal of Sound and Vibration*, 26(1):159–160.

[16] Strømmen, E. (2010). *Theory of bridge aerodynamics*. Springer Science & Business Media.

[17] Strømmen, E. (2013). *Structural Dynamics*. Springer Science & Business Media.

[18] Sumner, D., Richards, M., and Akosile, O. (2008). Strouhal number data for two staggered circular cylinders. *Journal of Wind Engineering and Industrial Aerodynamics*, 96(6):859–871.

[19] Takahashi, K. (1981). An approach to investigate the instability of the multiple-degree-of-freedom parametric dynamic systems. *Journal of sound and Vibration*, 78(4):519–529.

[20] Takahashi, K. (1991). Dynamic stability of cables subjected to an axial periodic load. *Journal of Sound and Vibration*, 144(2):323–330.

[21] Trethewey, M. and Cafeo, J. (1992). Tutorial: signal processing aspects of structural impact testing. *The International Journal of Analytical and Experimental Modal Analysis*, 7(2):129–149.

[22] Trivellato, F. and Castelli, M. R. (2015). Appraisal of strouhal number in wind turbine engineering. *Renewable and Sustainable Energy Reviews*, 49:795–804.

[23] Vegvesen, S. (2011). Hardangerbrua, teknisk brosjyre. [Online; accessed 5-February-2016].

[24] Vistnes, A. (2013). *Svingninger og bølger*. Kurland: A.I. Vistnes.

[25] Wójcicki, Z. and Bryja, D. (2014). Unusual combination parametric resonance. *Procedia Engineering*, 91:154–159.

Appendix A

Additional Information on Hangers

Presented in Appendix A are additional information on the hangers. Included are characteristics for all hangers and extracted frequencies, both numerical and from modal analyses.

A.1 Hanger Characteristics

Characteristics like length, pin to pin, and tension for all 30 hangers are listed in table A.1. Information is retrieved from the technical drawings provided by the Norwegian Public Roads Administration [1].

	Characteristic	
Hanger	Length [m]	Tension [kN]
1	126.231	980
2	118.449	983
3	110.933	877
4	103.668	882
5	96.655	881
6	89.893	881
7	83.382	881
8	77.121	881
9	71.109	881
10	65.347	881
11	59.833	881
12	54.567	881
13	49.550	881
14	44.779	881
15	40.256	881
16	35.979	881
17	31.948	881
18	28.164	881
19	24.625	881
20	21.331	881
21	18.283	881
22	15.479	881
23	12.921	881
24	10.606	881
25	8.536	881
26	6.710	881
27	5.128	881
28	3.790	881
29	2.695	881
30	1.845	881

Table A.1: Hanger characteristics - length and tension

A.2 Natural Frecuencies Extracted from Abaqus

First 20 natural frequencies for the 30 hangers are presented in table A.2, A.3 and A.4. Hangers are modelled with properties as listed in table 4.1 in chapter 4 and A.1.

	Mode						
Hanger	1	2	3	4	5	6	7
1	0.774	1.549	2.322	3.096	3.868	4.640	5.410
2	0.826	1.652	2.477	3.302	4.126	4.949	5.770
3	0.835	1.670	2.504	3.338	4.171	5.003	5.834
4	0.895	1.790	2.685	3.579	4.472	5.364	6.255
5	0.959	1.917	2.876	3.833	4.790	5.745	6.699
6	1.030	2.060	3.089	4.117	5.145	6.171	7.196
7	1.109	2.218	3.326	4.434	5.541	6.646	7.749
8	1.198	2.395	3.592	4.788	5.983	7.176	8.368
9	1.297	2.594	3.890	5.186	6.480	7.772	9.063
10	1.409	2.818	4.227	5.634	7.040	8.444	9.847
11	1.536	3.072	4.608	6.142	7.675	9.206	10.735
12	1.681	3.362	5.042	6.721	8.399	10.074	11.747
13	1.847	3.694	5.540	7.384	9.227	11.068	12.907
14	2.038	4.076	6.113	8.149	10.183	12.215	14.243
15	2.260	4.520	6.779	9.036	11.292	13.544	15.794
16	2.520	5.039	7.557	10.073	12.587	15.099	17.607
17	2.825	5.650	8.473	11.295	14.114	16.931	19.743
18	3.188	6.375	9.561	12.746	15.928	19.107	22.282
19	3.623	7.246	10.867	14.486	18.102	21.717	25.326
20	4.150	8.300	12.449	16.595	20.739	24.881	29.019
21	4.796	9.592	14.387	19.180	23.970	28.759	33.543
22	5.598	11.196	16.792	22.388	27.983	33.574	39.163
23	6.605	13.210	19.815	26.420	33.025	39.630	46.233
24	7.890	15.780	23.671	31.565	39.462	47.365	55.270
25	9.550	19.103	28.661	38.226	47.799	57.386	66.987
26	11.728	23.461	35.207	46.971	58.758	70.576	82.428
27	14.615	29.243	43.900	58.596	73.345	88.162	103.059
28	18.459	36.948	55.497	74.134	92.892	111.797	130.878
29	23.523	47.111	70.830	94.745	118.917	143.411	168.290
30	29.891	59.919	90.223	120.937	152.195	184.126	216.849

Table A.2: Extracted natural frequencies [Hz], mode 1-7

	Mode						
Hanger	8	9	10	11	12	13	14
1	6.179	6.946	7.712	8.503	9.267	10.029	10.789
2	6.591	7.409	8.226	9.070	9.885	10.698	11.508
3	6.663	7.491	8.317	9.140	9.962	10.781	11.598
4	7.144	8.032	8.918	9.801	10.682	11.561	12.436
5	7.652	8.602	9.551	10.497	11.441	12.381	13.319
6	8.219	9.240	10.259	11.275	12.289	13.300	14.307
7	8.851	9.951	11.048	12.143	13.234	14.323	15.408
8	9.558	10.745	11.930	13.112	14.291	15.467	16.638
9	10.352	11.638	12.921	14.201	15.478	16.751	18.021
10	11.247	12.644	14.039	15.430	16.818	18.201	19.579
11	12.262	13.785	15.305	16.823	18.335	19.843	21.347
12	13.418	15.085	16.749	18.409	20.065	21.715	23.362
13	14.742	16.574	18.403	20.227	22.046	23.861	25.670
14	16.269	18.292	20.310	22.323	24.332	26.334	28.331
15	18.040	20.283	22.522	24.755	26.983	29.205	31.420
16	20.112	22.613	25.108	27.599	30.083	32.562	35.033
17	22.552	25.357	28.156	30.951	33.738	36.518	39.292
18	25.452	28.618	31.778	34.935	38.081	41.223	44.356
19	28.931	32.533	36.127	39.716	43.298	46.871	50.438
20	33.150	37.279	41.401	45.517	49.626	53.729	57.823
21	38.325	43.099	47.871	52.636	57.394	62.147	66.893
22	44.750	50.333	55.913	61.488	67.060	72.627	78.188
23	52.838	59.441	66.045	72.648	79.251	85.855	92.458
24	63.180	71.096	79.020	86.953	94.893	102.843	110.804
25	76.606	86.243	95.904	105.588	115.300	125.040	134.815
26	94.322	106.263	118.260	130.314	142.436	154.629	166.906
27	118.052	133.151	148.369	163.723	179.224	194.869	210.705
28	150.166	169.691	189.474	209.543	229.931	250.653	271.757
29	193.612	219.427	245.799	272.792	300.453	328.830	357.971
30	250.494	285.158	320.968	358.019	396.407	436.212	477.528

Table A.3: Extracted natural frequencies [Hz], mode 8-14

	Mode					
Hanger	15	16	17	18	19	20
1	11.546	12.300	13.051	13.799	14.544	15.285
2	12.315	13.120	13.921	14.719	15.513	16.304
3	12.412	13.223	14.030	14.834	15.635	16.431
4	13.309	14.178	15.044	15.907	16.765	17.620
5	14.254	15.185	16.113	17.036	17.956	18.871
6	15.311	16.312	17.308	18.301	19.288	20.272
7	16.488	17.566	18.640	19.708	20.773	21.831
8	17.806	18.970	20.130	21.284	22.433	23.577
9	19.286	20.547	21.803	23.052	24.297	25.536
10	20.954	22.325	23.689	25.048	26.401	27.747
11	22.847	24.340	25.828	27.309	28.786	30.255
12	25.002	26.638	28.266	29.889	31.505	33.112
13	27.473	29.270	31.061	32.843	34.619	36.388
14	30.322	32.305	34.284	36.252	38.213	40.166
15	33.629	35.831	38.024	40.209	42.386	44.554
16	37.497	39.953	42.400	44.840	47.269	49.690
17	42.057	44.815	47.562	50.301	53.030	55.747
18	47.481	50.597	53.702	56.799	59.885	62.960
19	53.995	57.544	61.082	64.611	68.128	71.634
20	61.908	65.984	70.050	74.107	78.153	82.188
21	71.629	76.359	81.080	85.792	90.494	95.187
22	83.746	89.295	94.842	100.381	105.914	111.442
23	99.061	105.665	112.269	118.873	125.479	132.086
24	118.776	126.762	134.760	142.775	150.804	158.849
25	144.624	154.473	164.359	174.291	184.270	194.296
26	179.256	191.702	204.244	216.880	229.629	242.504
27	226.716	242.934	259.359	275.991	292.877	309.986
28	293.243	315.159	337.504	360.327	383.627	407.453
29	387.924	418.737	450.440	483.099	516.728	551.376
30	520.437	565.000	611.298	659.395	709.322	719.985

Table A.4: Extracted natural frequencies [Hz], mode 15-20

A.3 Natural Frequencies Extracted from MATLAB

The tables presented in this section visualize the natural frequencies extracted with CF and LF in MATLAB. Each frequency corresponds to the computed frequency for every hit location at the two hangers. Mean and standard deviation for the results also presented.

A.3.1 Circle Fit

	Hanger 1						
Mode	x-direction					μ	σ
1	0.753	0.755	0.754	0.776	NaN	0.760	0.0096
2	1.533	1.552	1.530	1.535	1.539	1.538	0.0079
3	2.322	2.332	2.324	2.317	2.330	2.325	0.0055
4	3.101	3.094	3.089	3.093	3.091	3.094	0.0040
5	3.874	3.874	3.867	3.866	3.863	3.869	0.0043
6	4.652	4.653	4.645	4.645	4.641	4.647	0.0048
7	5.433	5.435	5.425	5.422	5.419	5.427	0.0063
8	6.214	6.212	6.204	6.201	6.198	6.206	0.0061
9	6.999	6.998	6.991	6.985	6.982	6.991	0.0066
10	7.782	7.782	7.776	7.770	7.768	7.775	0.0060

Table A.5: Natural frequencies with mean and standard deviation from Hanger 1 in x-direction

	Hanger 1						
Mode	z-direction					μ	σ
1	0.787	0.751	0.778	0.784	0.759	0.772	0.0143
2	1.538	1.538	1.537	1.532	1.536	1.536	0.0022
3	2.312	2.305	2.306	2.297	2.300	2.304	0.0051
4	3.078	3.070	3.072	3.064	3.076	3.072	0.0049
5	3.845	3.840	3.841	3.842	3.840	3.842	0.0021
6	4.644	4.643	4.638	4.636	4.638	4.640	0.0033
7	5.384	5.377	5.377	5.374	5.371	5.377	0.0044
8	6.164	6.159	6.154	6.153	6.152	6.156	0.0046
9	6.983	6.981	6.985	6.984	6.981	6.983	0.0017
10	7.787	7.778	7.779	7.792	7.804	7.788	0.0097

Table A.6: Natural frequencies with mean and standard deviation from Hanger 1 in z-direction

	Hanger 2						
Mode	x-direction					μ	σ
1	0.765	0.789	0.818	0.776	NaN	0.787	0.0198
2	1.584	1.584	1.581	1.584	1.595	1.586	0.0048
3	2.375	2.376	2.373	2.374	2.365	2.373	0.0038
4	3.163	3.161	3.166	3.166	3.165	3.164	0.0019
5	3.959	3.960	3.959	3.955	3.954	3.957	0.0020
6	4.756	4.760	4.756	4.755	4.749	4.755	0.0034
7	5.552	5.555	5.553	5.551	5.550	5.552	0.0016
8	6.352	6.356	6.352	6.352	6.346	6.352	0.0034
9	7.155	7.158	7.157	7.157	7.159	7.157	0.0012
10	7.963	7.956	7.960	7.960	7.958	7.959	0.0024

Table A.7: Natural frequencies with mean and standard deviation from Hanger 2 in x-direction

	Hanger 2						
Mode	z-direction					μ	σ
1	0.795	0.777	0.769	0.781	0.764	0.777	0.0105
2	1.581	1.570	1.580	1.575	1.570	1.575	0.0048
3	2.360	2.360	2.359	2.354	2.371	2.361	0.0056
4	3.151	3.155	3.150	3.153	3.132	3.148	0.0084
5	3.928	3.929	3.934	3.927	3.942	3.932	0.0055
6	4.702	4.714	4.707	4.699	4.703	4.705	0.0050
7	5.639	5.629	5.638	5.620	5.622	5.630	0.0080
8	6.418	6.413	6.412	6.419	6.413	6.415	0.0028
9	7.199	7.219	7.215	7.204	7.229	7.213	0.0108
10	7.960	7.956	7.958	7.955	7.954	7.957	0.0020

Table A.8: Natural frequencies with mean and standard deviation from Hanger 2 in z-direction

A.3.2 Line Fit

	Hanger 1						
Mode	x-direction					μ	σ
1	0.764	0.768	0.757	0.770	0.723	0.756	0.0174
2	1.542	1.544	1.545	1.541	1.541	1.543	0.0019
3	2.320	2.322	2.320	2.320	2.323	2.321	0.0010
4	3.097	3.094	3.092	3.094	3.094	3.094	0.0014
5	3.872	3.872	3.870	3.870	3.869	3.871	0.0011
6	4.649	4.649	4.647	4.647	4.645	4.647	0.0014
7	5.429	5.430	5.427	5.426	5.425	5.427	0.0019
8	6.209	6.208	6.207	6.206	6.204	6.207	0.0017
9	6.996	6.995	6.994	6.993	6.991	6.994	0.0019
10	7.779	7.779	7.778	7.776	7.775	7.777	0.0018

Table A.9: Natural frequencies with mean and standard deviation from Hanger 1 in x-direction

	Hanger 1						
Mode	z-direction					μ	σ
1	0.777	0.768	0.773	0.765	0.769	0.770	0.0042
2	1.539	1.539	1.540	1.536	1.546	1.540	0.0035
3	2.306	2.304	2.305	2.301	2.301	2.303	0.0020
4	3.077	3.071	3.072	3.070	3.073	3.073	0.0023
5	3.842	3.846	3.848	3.846	3.845	3.845	0.0018
6	4.648	4.646	4.645	4.644	4.644	4.645	0.0014
7	5.377	5.380	5.380	5.378	5.378	5.378	0.0011
8	6.164	6.162	6.160	6.161	6.161	6.162	0.0015
9	6.989	6.987	6.990	6.990	6.988	6.989	0.0012
10	7.793	7.782	7.789	7.793	7.799	7.791	0.0056

Table A.10: Natural frequencies with mean and standard deviation from Hanger 1 in z-direction

	Hanger 2						
Mode	x-direction					μ	σ
1	0.795	0.786	0.824	0.788	0.789	0.796	0.0141
2	1.585	1.585	1.584	1.584	1.583	1.584	0.0009
3	2.373	2.374	2.373	2.373	2.375	2.373	0.0008
4	3.162	3.168	3.168	3.168	3.168	3.167	0.0023
5	3.958	3.958	3.957	3.957	3.961	3.958	0.0013
6	4.757	4.758	4.758	4.757	4.756	4.757	0.0006
7	5.555	5.556	5.555	5.554	5.554	5.555	0.0006
8	6.356	6.357	6.356	6.356	6.354	6.356	0.0008
9	7.160	7.156	7.160	7.160	7.160	7.159	0.0018
10	7.966	7.958	7.964	7.965	7.963	7.963	0.0027

Table A.11: Natural frequencies with mean and standard deviation from Hanger 2 in x-direction

	Hanger 2						
Mode	z-direction					μ	σ
1	0.785	0.780	0.776	0.781	0.774	0.779	0.0039
2	1.572	1.572	1.574	1.573	1.572	1.573	0.0009
3	2.360	2.360	2.359	2.358	2.361	2.360	0.0009
4	3.149	3.145	3.148	3.150	3.147	3.148	0.0016
5	3.938	3.930	3.932	3.930	3.935	3.933	0.0032
6	4.707	4.712	4.710	4.708	4.709	4.709	0.0018
7	5.637	5.629	5.631	5.626	5.624	5.629	0.0046
8	6.420	6.418	6.418	6.416	6.418	6.418	0.0015
9	7.209	7.218	7.215	7.212	7.224	7.216	0.0050
10	7.962	7.961	7.962	7.960	7.960	7.961	0.0007

Table A.12: Natural frequencies with mean and standard deviation from Hanger 2 in z-direction

Appendix B

Additional Details from Fieldwork

Following in this appendix are detailed descriptions of the measurements executed on the Hardanger Bridge and the MATLAB scripts to process the signals. Files are saved in folder *Fieldwork*. Sub-folder *Measurements Original* and *Measurements Global* contains the original MAT.files and processed MAT.files, respectively. The processed MAT.files are divided up in separate folders for each accelerometer containing the MAT.files with the data, while the original MAT.files contains data for all accelerometers combined. Various photos from the excursion are saved in sub-folder *Photos*. The global directions for all measurements are demonstrated in figure B.1. All accelerometers where installed in global directions except for the accelerometer mounted on the hangers, see section B.1.1. In sub-folder *20160331_1041 Passing traffic* under folder *Measurements Original*, information about passing traffic is saved. The folder includes photos of passing cars and information regarding when cars drove on and off the bridge. The MATLAB scripts for the hammer tests are saved in subfolder *EasyMod toolbox* under the folder *MATLAB Scripts*. The subfolder *SensorsDatabase* contains information of each accelerometer and the modal hammer, like serial number and sensitivity.

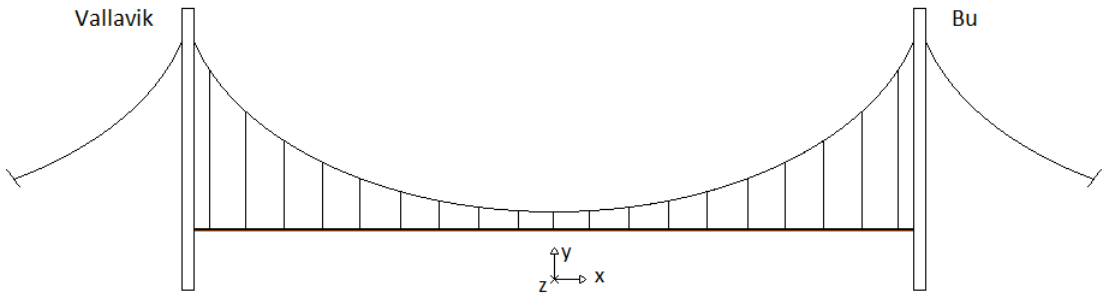

Figure B.1: Global coordinate system

B.1 Hammer Tests

B.1.1 Accelerometer on Hangers

The accelerometers on a hanger were mounted on a open steel cylinder which again was mounted to the hanger. Local coordinate axis are demonstrated in figure B.2. Decomposition of local axis into global axis are shown in figure B.3. Blue axis represent the accelerometers local axis and black axis the global axis.

Figure B.2: Accelerometer mounted to steel section

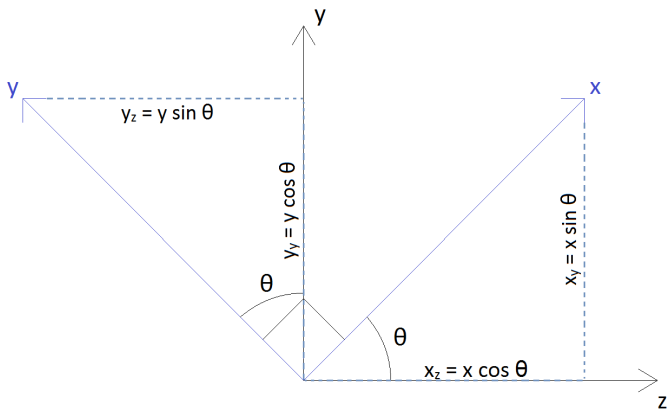

Figure B.3: Decomposition of accelerometer mounted on hanger

B.1.2 Original Signals

Original measurements from each set up are saved in MATLAB.files, containing data from hammer and accelerometer. The signals are named *Test1-loc1-no1* where *loc1* refer to hit location and *no1* refer to which hit out of three hits at location 1. For the hammer tests on the hangers the files refer to ten locations corresponding to five coordinates. Odd location numbers represents hits in x-direction for the five successive coordinates and even location numbers equivalent for z-direction. Each MATLAB.file contain a matrix *data*, a vector *time* and a time stamp. For the hammer tests the data in the MATLAB.files contain ten columns. Where the first column is the hammer signal, while the next three columns are signals from accelerometer 1 in local x-, y- and z-direction, respectively, and so on for accelerometer 2 and 3. The data from the ambient signals are similar, only without the hammer signal in the first column, thus nine columns in total.

B.1.3 Hanger 1

MATLAB.files for measurements on Hanger 1 are saved in sub-folder *20160330_1143 Hanger01*. With reference to figure B.4, the coordinates for the accelerometer are listed in table B.1. Hit locations on Hanger 1 are marked with red stars and coordinates are listed in table B.2.

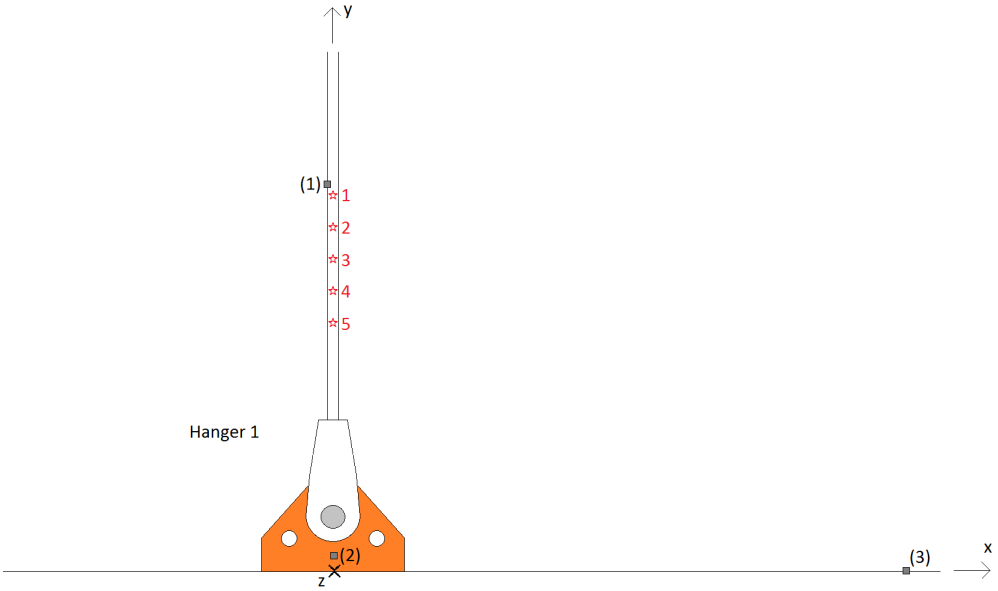

Figure B.4: Setup Hanger 1

Accelerometer		Hanger 1	
(1)	0.00	12.50	0.00
(2)	0.00	0.15	0.00
(3)	9.54	0.00	0.00
Local coord. [m]	x	y	z

Table B.1: Coordinates for accelerometers

Hit loc.		Hanger 1	
1	0.00	12.40	0.00
2	0.00	10.50	0.00
3	0.00	8.50	0.00
4	0.00	6.50	0.00
5	0.00	4.50	0.00
Local coord. [m]	x	y	z

Table B.2: Coordinates for hit locations on Hanger 1

B.1.4 Hanger 2

MATLAB.files for measurements on Hanger 2 are saved in sub-folder *20160330_1444 Hanger02*. With reference to figure B.5, the coordinates for the accelerometer are listed in table B.3. Hit locations on Hanger 2 are marked with red stars and coordinates are listed in table B.4.

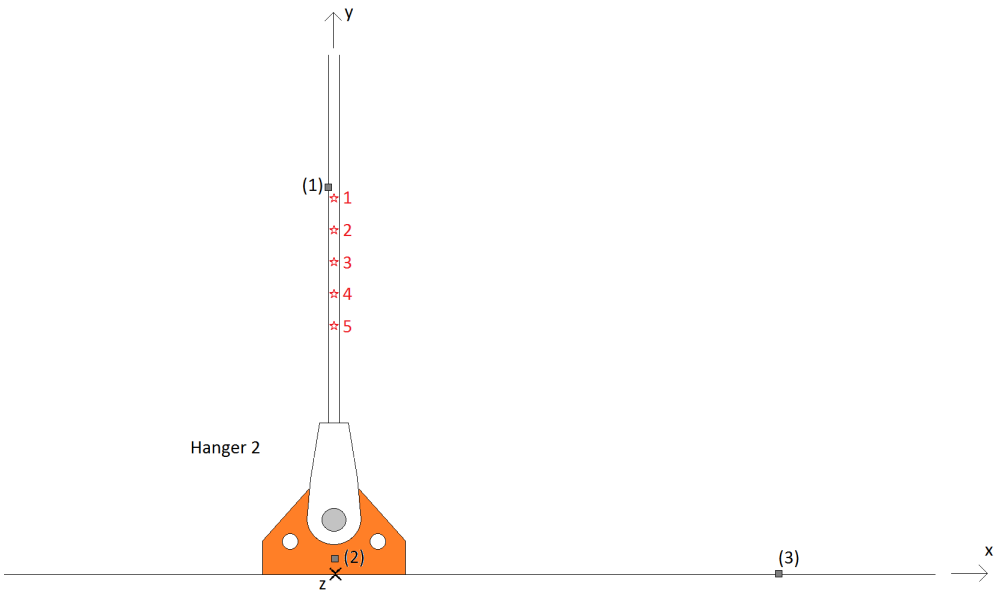

Figure B.5: Setup Hanger 2

Accelerometer		Hanger 2	
(1)	0.00	12.35	0.00
(2)	0.00	0.15	0.00
(3)	9.60	0.00	0.00
Local coord. [m]	x	y	z

Table B.3: Coordinates for accelerometers

Hit loc.		Hanger 2	
1	0.00	12.21	0.00
2	0.00	10.35	0.00
3	0.00	8.35	0.00
4	0.00	6.35	0.00
5	0.00	4.35	0.00
Local coord. [m]	x	y	z

Table B.4: Coordinates for hit locations on Hanger 2

B.1.5 Girder 1

MATLAB.files for measurements on Girder 1 are saved in sub-folder *20160330_1122 Girder01*. With reference to figure B.6, the coordinates for the accelerometer are listed in table B.5. Hit locations on Girder 1 are marked with blue stars and coordinates are listed in table B.6.

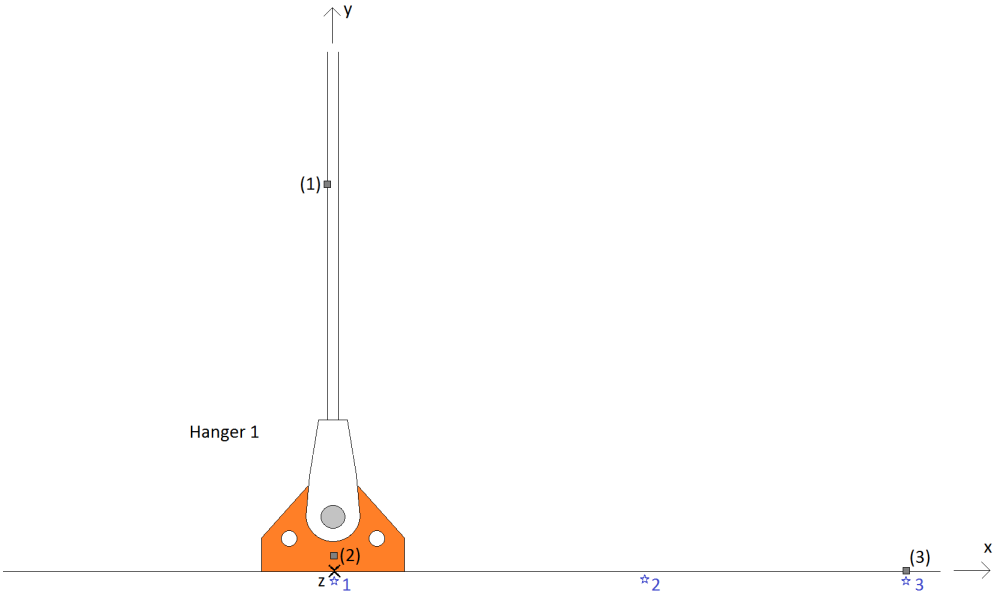

Figure B.6: Setup Girder 1

Accelerometer		Girder 1	
(1)	0.00	12.50	0.00
(2)	0.00	0.15	0.00
(3)	9.54	0.00	0.00
Local coord. [m]	x	y	z

Table B.5: Coordinates for accelerometers

Hit loc.		Girder 1	
1	0.00	0.00	0.00
2	4.42	0.00	0.00
3	9.54	0.00	0.00
Local coord. [m]	x	y	z

Table B.6: Coordinates for hit locations on Girder 1

B.1.6 Girder 2

MATLAB.files for measurements on Girder 2 are saved in sub-folder *20160330_1546 Girder02*. With reference to figure B.7, the coordinates for the accelerometer are listed in table B.7. Hit locations on Girder 2 are marked with blue stars and coordinates are listed in table B.8.

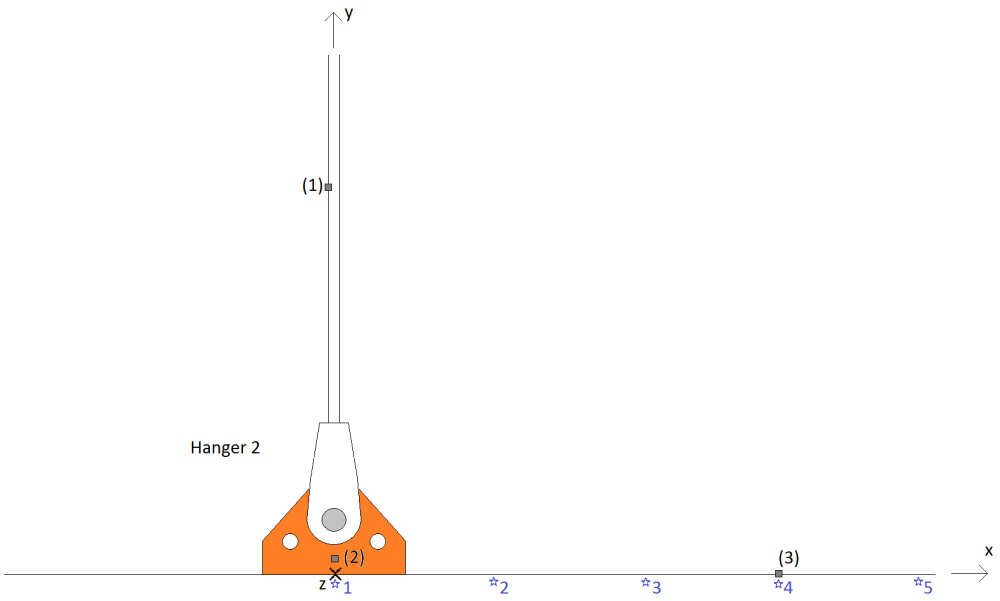

Figure B.7: Setup Girder 2

Accelerometer		Girder 2	
(1)	0.00	12.50	0.00
(2)	0.00	0.15	0.00
(3)	9.54	0.00	0.00
Local coord. [m]	x	y	z

Table B.7: Coordinates for accelerometers

Hit loc.		Girder 2	
1	0.00	0.00	0.00
2	3.50	0.00	0.00
3	6.50	0.00	0.00
4	9.60	0.00	0.00
5	12.40	0.00	0.00
Local coord. [m]	x	y	z

Table B.8: Coordinates for hit locations on Girder 2

B.2 Ambient Vibrations

B.2.1 Hanger 1 - Day 1

MATLAB.files for ambient vibrations on Hanger 1 the first day are saved in sub-folder *20160330_1259 Ambiend vibration Hanger01*. With reference to figure B.8, the coordi-

nates for the accelerometer are listed in table B.9.

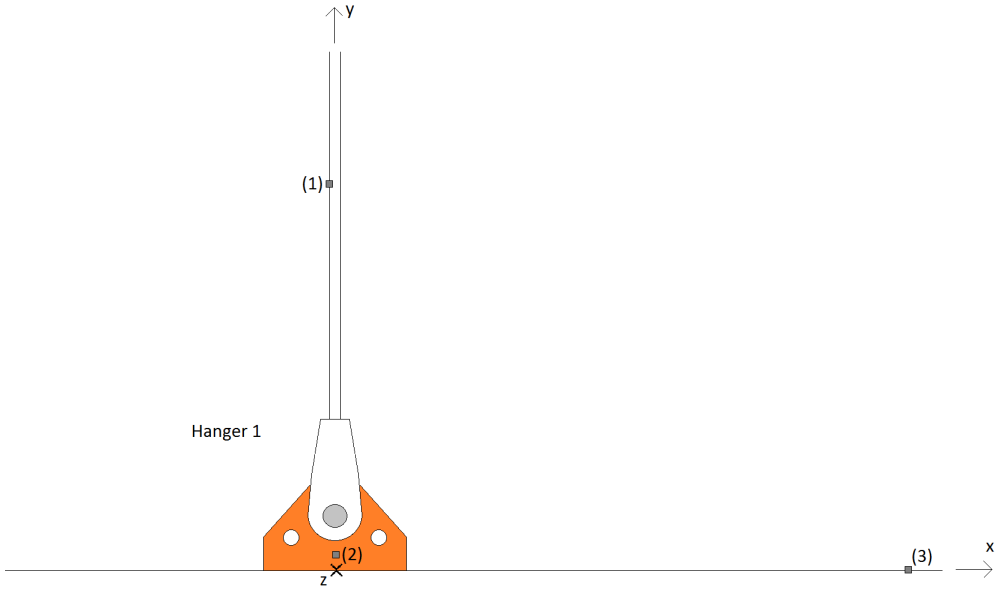

Figure B.8: Setup for ambient vibrations on Hanger 1 - Day 1

Accelerometer		Hanger 1	
(1)	0.00	12.50	0.00
(2)	0.00	0.15	0.00
(3)	9.54	0.00	0.00
Local coord. [m]	x	y	z

Table B.9: Coordinates for accelerometers

B.2.2 Hanger 1 - Day 2

MATLAB.files for ambient vibrations on Hanger 1 the second day are saved in sub-folder *20160331_1035 Ambiend vibration Hanger01*. With reference to figure B.9, the coordinates for the accelerometer are listed in table B.10.

Accelerometer		Hanger 1	
(1)	0.00	1.70	0.00
(2)	0.00	0.55	0.00
(3)	0.00	0.15	0.00
Local coord. [m]	x	y	z

Table B.10: Coordinates for accelerometers

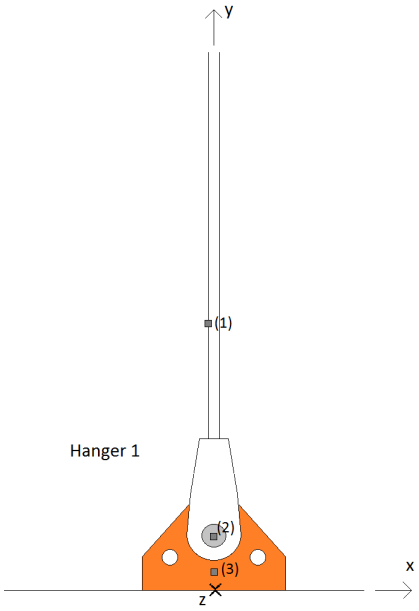

Figure B.9: Setup for ambient vibrations on Hanger 1 - Day 2

B.2.3 Hanger 2

MATLAB.files for ambient vibrations on Hanger 2 are saved in sub-folder *20160331_1301 Ambiend vibration Hanger02*. With reference to figure B.10, the coordinates for the accelerometer are listed in table B.11.

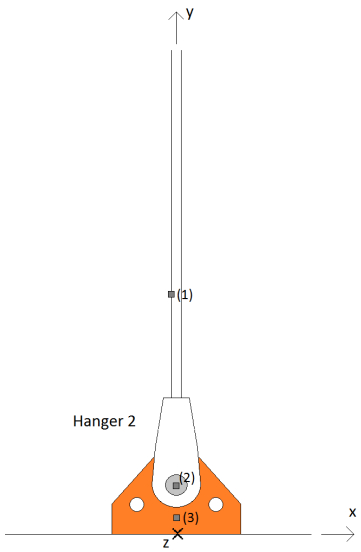

Figure B.10: Setup for ambient vibrations on Hanger 2

Accelerometer		Hanger 2	
(1)	0.00	1.65	0.00
(2)	0.00	0.56	0.00
(3)	0.00	0.20	0.00
Local coord. [m]	x	y	z

Table B.11: Coordinates for accelerometers

B.2.4 Girder 0

MATLAB.files for ambient vibrations on Girder 0 are saved in sub-folder *20160331_0905 Ambiend vibration Girder00*. With reference to figure B.11, the coordinates for the accelerometer are listed in table B.12.

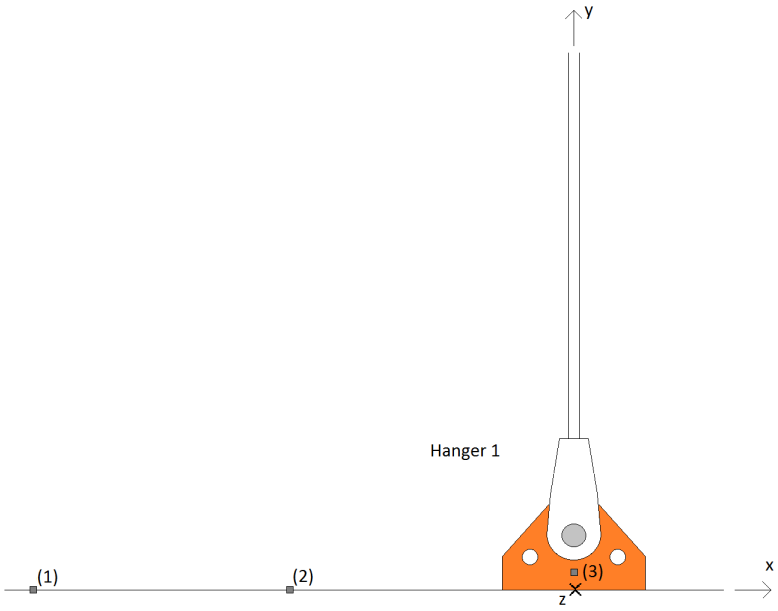

Figure B.11: Setup for ambient vibrations on Girder 0

Accelerometer		Girder 0	
(1)	-8.56	0.00	0.00
(2)	-4.57	0.00	0.00
(3)	0.00	0.15	0.00
Local coord. [m]	x	y	z

Table B.12: Coordinates for accelerometers

B.2.5 Girder 1

MATLAB.files for ambient vibrations on Girder 1 are saved in sub-folder *20160331_1154 Ambiend vibration Girder01*. With reference to figure B.12, the coordinates for the accelerometer are listed in table B.13.

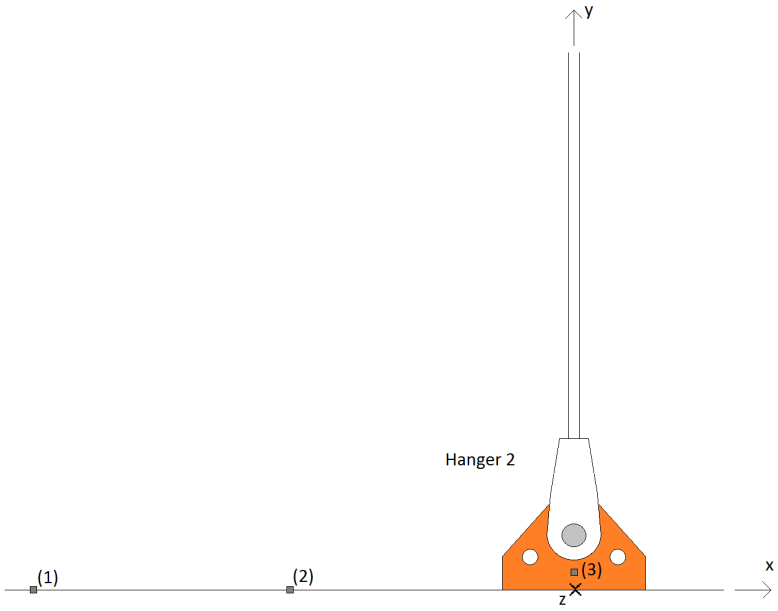

Figure B.12: Setup for ambient vibrations on Girder 1

Accelerometer		Girder 1	
(1)	-12.60	0.00	0.00
(2)	-6.60	0.00	0.00
(3)	0.00	0.20	0.00
Local coord. [m]	x	y	z

Table B.13: Coordinates for accelerometers

B.3 Signal Processing

This section is provided to give the reader and user of the MATLAB program further information about the EasyMod toolbox. EasyMod toolbox is a MATLAB program to extract dynamic properties of a structure on the basis of the data from modal hammer tests. The program is an open source program, and modifications with supplemental functions and scripts are made by Postdoc Daniel Cantero. The necessary information

regarding how to implement the input is in the script *A00_ToDo.m*. *A01_dataLogger.m* is the main script when generating the input with the modal hammer. All the necessary information of the setup must be inputted here. Coordinates of the accelerometers and hit locations, number of hits and duration of each signal must be fed in. *A02b_signalAnalysis_withEasyMod.m* is the main script for the output. Three different methods to extract the dynamic properties are used in this toolbox, and the user can specify which of the methods to use:

- CF
- LF
- LSCE

Appendix C

MATLAB Scripts

In this appendix some of the MATLAB scripts utilized in this thesis are presented.

C.1 Modelling Hangers in Abaqus

Main script and supplementing scripts:

- *Hanger_no.m*
- *Nodes.m*
- *Elements.m*

Hanger_no.m models the hangers as described in the technical drawings provided by the Norwegian Public Roads Administration and steel properties. Supplementing scripts are described in C.3.

C.2 Modelling PE

Main script and supplementing scripts:

- *PE_cable.m*
- *Nodes.m*
- *Elements.m*

- *Damping.m*

PE_cable.m models a cable with similar properties as the hangers and extracts natural frequencies before applying a moving BC to excite PE.

C.3 Supplementing Scripts

Supplementing script to the main scripts presented earlier in the appendix. *Nodes.m* generates nodes and *Elements.m* generates elements. *Damping.m* calculates the α and β coefficient in Rayleigh Damping, see 2.4.

Hanger_no.m

Contents

- Input
- Geometry
- Create input file
- Preprint
- Nodes
- Elements
- Create section
- Step1: Temperture step - pretensioning
- Static step2: Frequency step - eigenfrequencies
- Run analysis

```
function [] = Hanger_no(i)
```

Input

```
————————————————- Input————————————————-

L=[127.531 119.749 112.233 104.968 97.955 91.193 84.682 78.421...
72.409 66.647 61.133 55.867 50.850 46.079 41.556 37.279 33.248...
29.464 25.925 22.631 19.583 16.779 14.221 11.906 9.836 8.010...
6.428 5.090 3.995 3.145];
L=L(i); % [m]

Emodul=160e9;               % E-modulus
Gmodul=Emodul/(2*(1+0.3));  % G-modulus
alpha=1.2e-5;               % Thermal expancion coefficient
areal=0.0032;               % Section area [m^2]
density=7850;               % density [kg/m^3]
N_fr=20; % # requested natural frequencies
```

```
Load=881e3;                 % Tension [N]
if i==1
    Load=980e3;
end % if i==1
if i==2
    Load=983e3;
end %if i==2
if i==3
    Load=877e3;
end %if i==3
if i==4
    Load=882e3;
end % if i==3
temp=-Load/(areal*alpha*Emodul);
% pre-tensioning obtained by applying temperature to induce thermal...
% stresses
```

Geometry

```
elem=100;                   % # elements
disp=0;
```

———————————- Calculations ———————————-

Create input file

```
fid=fopen(['Hanger_no_' num2str(i) '.inp'],'wt');
```

Preprint

```
fprintf(fid, ['** \n']);
fprintf(fid, ['*PREPRINT, ECHO=YES, MODEL=YES, HISTORY=YES \n']);
fprintf(fid, ['** \n']);
```

Nodes

Cable nodes

```
fprintf(fid, ['** \n']);
fprintf(fid, ['** CableNodes \n']);
fprintf(fid, ['*NODE, NSET=hangernodes \n']);

nodes(L,elem,disp);
% generate nodes; L = lenght of beam,
% elem = # elements, disp = displacement at end node

fprintf(fid, ['*INCLUDE, INPUT=nodes.inp \n']);
```

Elements

Cable Elements

```
fprintf(fid, ['** \n']);
fprintf(fid, ['** CableElements \n']);
fprintf(fid, ['*ELEMENT, TYPE=B21, ELSET=HANGER \n']);

elements(elem); % generate elements, # elements

fprintf(fid, ['*INCLUDE, INPUT=elements.inp \n']);
```

Create section

Hanger Section

```
fprintf(fid, ['*BEAM GENERAL SECTION, ELSET=HANGER, SECTION=...'
              'GENERAL, DENSITY=' num2str(density) ' \n']);
fprintf(fid, [num2str(areal) ', 0.9E-8, 0, 0.9E-8,'...
              ' 1.86E-8 \n']); %areal,Iy,Iyz,Iz,Ir
```

```
fprintf(fid, ['0, 0, -1 \n']);
fprintf(fid, [num2str(Emodul) ', ' num2str(Gmodul) ', '...
              num2str(alpha) ' \n']); % E, G, alpha temp
```

Step1: Temperture step - pretensioning

```
fprintf(fid, ['** \n']);
fprintf(fid, ['*STEP, AMPLITUDE=STEP, INC=5000, NLGEOM \n']);
fprintf(fid, ['*STATIC \n']);
fprintf(fid, ['1, 1, 1e-5, 1 \n']);
fprintf(fid, ['*TEMPERATURE \n']);
fprintf(fid, ['hangernodes, ' num2str(temp) ' \n']);

% BC Cable
fprintf(fid, ['** \n']);
fprintf(fid, ['*BOUNDARY, OP=NEW \n']);
fprintf(fid, ['1, 1, 2 \n']);
fprintf(fid, [ num2str(elem+1) ', 1, 2  \n']); % BC at end node

%End step1
fprintf(fid, ['** \n']);
fprintf(fid, ['*END STEP \n']);
fprintf(fid, ['** \n']);
```

Static step2: Frequency step - eigenfrequencies

```
fprintf(fid, ['** \n']);
fprintf(fid, ['*STEP, AMPLITUDE=RAMP, INC=5000, NLGEOM \n']);
fprintf(fid, ['*FREQUENCY, NORMALIZATION=DISPLACEMENT \n']);
fprintf(fid, [ num2str(N_fr) ' \n']);
fprintf(fid, ['** \n']);
```

```
fprintf(fid, ['*OUTPUT, FIELD \n']);
fprintf(fid, ['*NODE OUTPUT, NSET=hangernodes \n']);
fprintf(fid, ['U \n']);

fprintf(fid, ['*OUTPUT, FIELD \n']);
fprintf(fid, ['*ELEMENT OUTPUT, ELSET=HANGER \n']);
fprintf(fid, ['S \n']);

%End step2
fprintf(fid, ['** \n']);
fprintf(fid, ['*END STEP \n']);
fprintf(fid, ['** \n']);
```

Run analysis

```
clc
JobName=['Hanger_no_' num2str(i)]
system(['abaqus job=' JobName ' input=Hanger_no_' num2str(i) ...
        ' interactive'])

pause(2)

winopen([ JobName '.odb']);

end
```

PE_Cable.m

Contents

Input

```
————————————Input————————————

L=100;              % cable length [m]
eig=5.9146;         % cable's eigenfrequency [rad/time]
T=20;               % T - Total time step
amp=0.10;           % BC displacement [m]
elem=100;           % # elements
N_fr=20;            % # requested natural frequencies

Emodul=160e9;               % E-modulus
Gmodul=Emodul/(2*(1+0.3));  % G-modulus
alpha=1.2e-5;               % Thermal expancion coefficient
areal=0.0032;               % Section area [m^2]
density=7850;               % density [kg/m^3]
```

```
% ----------------------Calculations----------------------

exc_freq=eig*2;     % excitation frequency - 2x eigenfrequency
disp=L/100;          % inclinement on cable
```

Create input file

```
fid=fopen(['PE_cable.inp'],'wt');
```

Preprint

```
fprintf(fid, ['** \n']);
fprintf(fid, ['*PREPRINT, ECHO=YES, MODEL=YES, HISTORY=YES \n']);
fprintf(fid, ['** \n']);
```

Nodes

Cable nodes

```
fprintf(fid, ['** \n']);
fprintf(fid, ['** CableNodes \n']);
fprintf(fid, ['*NODE, NSET=hangernodes \n']);

Nodes(L,elem,disp);
% generate nodes;L = lenght of beam, elem = # elements,...
% disp = displacement at end node

fprintf(fid, ['*INCLUDE, INPUT=nodes.inp \n']);
```

Elements

Cable Elements

```
fprintf(fid, ['** \n']);
fprintf(fid, ['** CableElements \n']);
fprintf(fid, ['*ELEMENT, TYPE=B21, ELSET=HANGER \n']);

Elements(elem); % generate elements, # elements

fprintf(fid, ['*INCLUDE, INPUT=elements.inp \n']);
```

Create section

Hanger Section

```
fprintf(fid, ['*BEAM GENERAL SECTION, ELSET=HANGER, SECTION=...
              'GENERAL, DENSITY=' num2str(density) ' \n']);
fprintf(fid, [num2str(areal) ', 0.9E-8, 0, 0.9E-8,'...
              ' 1.86E-8 \n']);            % areal,Iy,Iyz,Iz,Ir
fprintf(fid, ['0, 0, -1 \n']);
fprintf(fid, [num2str(Emodul) ', ' num2str(Gmodul) ', '...
              num2str(alpha) ' \n']);     % E, G, alpha temp

fprintf(fid, ['*SECTION POINTS \n']); % need for input 'S' - stress
fprintf(fid, ['0, 0 \n']);            % x1, x2 in local coordinates
```

Damping

```
Damping(eig);
fprintf(fid, ['*INCLUDE, INPUT=Damping.inp \n']); %Reyleigh damping
```

Amplitude

```
fprintf(fid, ['** \n']);
fprintf(fid, ['*AMPLITUDE, NAME=Amp, DEFINITION=PERIODIC \n']);
fprintf(fid, ['1, ' num2str(exc_freq) ', 0, 0 \n']);
% frequency, starting time, initial amplitude
```

```
fprintf(fid, ['0, ' num2str(amp) ' \n']);
% cosinus term, sinusterm of fourier expansion
```

Step1: Temperture step - pretensioning

```
fprintf(fid, ['** \n']);
fprintf(fid, ['*STEP, AMPLITUDE=STEP, INC=5000, NLGEOM \n']);
fprintf(fid, ['*STATIC \n']);
fprintf(fid, ['1, 1, 1e-5, 1 \n']);
fprintf(fid, ['*TEMPERATURE \n']);
fprintf(fid, ['hangernodes, -144 \n']);

% BC Cable
fprintf(fid, ['** \n']);
fprintf(fid, ['*BOUNDARY, OP=NEW \n']);
fprintf(fid, ['1, 1, 2 \n']);
fprintf(fid, [num2str(elem+1) ', 1, 2  \n']);

%End step1
fprintf(fid, ['** \n']);
fprintf(fid, ['*END STEP \n']);
fprintf(fid, ['** \n']);
```

Static step2: Frequency step - eigenfrequencies

```
fprintf(fid, ['** \n']);
fprintf(fid, ['*STEP, AMPLITUDE=RAMP, INC=5000, NLGEOM \n']);
fprintf(fid, ['*FREQUENCY, NORMALIZATION=DISPLACEMENT \n']);
fprintf(fid, [ num2str(N_fr) ' \n']);
fprintf(fid, ['** \n']);

%Outputs
```

```
fprintf(fid, ['*OUTPUT, FIELD \n']);
fprintf(fid, ['*NODE OUTPUT, NSET=hangernodes \n']);
fprintf(fid, ['U \n']);

fprintf(fid, ['*OUTPUT, FIELD \n']);
fprintf(fid, ['*ELEMENT OUTPUT, ELSET=HANGER \n']);
fprintf(fid, ['S \n']);

%End step2
fprintf(fid, ['** \n']);
fprintf(fid, ['*END STEP \n']);
fprintf(fid, ['** \n']);
```

Static step3: Moving BC

```
fprintf(fid, ['** \n']);
fprintf(fid, ['*STEP, AMPLITUDE=RAMP, INC=10000, NLGEOM \n']);
fprintf(fid, ['*DYNAMIC \n']);
fprintf(fid, ['.1, ' num2str(T) ', 1e-5, 0.5 \n']);

% BC Cable
fprintf(fid, ['** \n']);
fprintf(fid, ['*BOUNDARY, AMPLITUDE=Amp, OP=MOD \n']);
fprintf(fid, [num2str(elem+1) ', 1, 1, 1 \n']);

fprintf(fid, ['*NSET, NSET=NODE_mid \n']);
fprintf(fid, [num2str(elem/4) ', ' num2str(elem/2) ', ...
             'num2str(3*elem/4) ' \n']);

fprintf(fid, ['*ELSET, ELSET=EL_mid \n']);
fprintf(fid, [num2str(elem/2) ' \n']);
```

```
% Output
fprintf(fid, ['*OUTPUT, FIELD, TIME INTERVAL=0.001  \n']);
fprintf(fid, ['*NODE OUTPUT, NSET=hangernodes \n']);
fprintf(fid, ['U \n']);

fprintf(fid, ['*OUTPUT, HISTORY \n']);
fprintf(fid, ['*NODE PRINT, NSET=NODE_mid \n']);
fprintf(fid, ['U \n']);

fprintf(fid, ['*OUTPUT, FIELD, TIME INTERVAL=0.002 \n']);
fprintf(fid, ['*ELEMENT OUTPUT, ELSET=HANGER \n']);
fprintf(fid, ['S \n']);

fprintf(fid, ['*OUTPUT, HISTORY \n']);
fprintf(fid, ['*EL PRINT, ELSET=EL_mid \n']);
fprintf(fid, ['S \n']);

%End step3
fprintf(fid, ['** \n']);
fprintf(fid, ['*END STEP \n']);
fprintf(fid, ['** \n']);
```

Run analysis

```
clc
JobName=['PE_cable']
system(['abaqus job=' JobName ' input=PE_cable interactive'])

pause(2)

winopen([ JobName '.odb']);
```

Nodes.m

```
function [ ] = Nodes( L,elem,disp)
%  L = length of beam, elem = # elements, disp = displacement
% in Y-dir.
fid=fopen('nodes.inp','wt');

e_l=L/elem;    % element length
inc=disp/L*e_l; % height inclinement per one element length

x_co=0;
y_co=0;

for i=1:elem+1 % # nodes
fprintf(fid, [num2str(i) ',' num2str(x_co) ',' num2str(y_co) '\n']);

    x_co=x_co+e_l;
    y_co=y_co+inc;

end
```

Elements.m

```
function [  ] = Elements( elem ) % creates elements;
% element #,node1,node2
fid=fopen('elements.inp','wt');

node=1;
for i=1:elem
fprintf(fid, [num2str(i) ',' num2str(node) ',' num2str(node+1) '\n']);

    node=node+1;

end
```

Rayleigh damping

```
function [ ] = damping(freq)    %freq = eigenfrequency*FR [rad/time]
fid=fopen('damping.inp','wt');

freq=freq/(2*pi);

% e1=% damping at f1=[Hz], e2=% damping at f2=[Hz]
e1=0.02; e2=0.02;
f1=freq; f2=freq*2;

om1=2*pi*f1;
om2=2*pi*f2;

alpha_beta=2*[1/om1 om1;1/om2 om2]^-1*[e1;e2]

fprintf(fid, ['*DAMPING, ALPHA=' num2str(alpha_beta(1,1))...
              ',BETA=' num2str(alpha_beta(2,1)) '\n']);
end
```